HHS Public Access

Author manuscript

Cell. Author manuscript; available in PMC 2018 June 29.

Published in final edited form as:

Cell. 2017 June 29; 170(1): 127–141.e15. doi:10.1016/j.cell.2017.06.016.

IFNγ-Dependent Tissue-Immune Homeostasis Is Co-opted in the Tumor Microenvironment

Christopher J. Nirschl[1,25], **Mayte Suárez-Fariñas**[2,3,4,25], **Benjamin Izar**[5,6,7], **Sanjay Prakadan**[5,8,9], **Ruth Dannenfelser**[10,11], **Itay Tirosh**[5], **Yong Liu**[1], **Qian Zhu**[10,11], **K. Sanjana P. Devi**[1], **Shaina L. Carroll**[5,8,9], **David Chau**[1], **Melika Rezaee**[12], **Tae-Gyun Kim**[1], **Ruiqi Huang**[3], **Judilyn Fuentes-Duculan**[13], **George X. Song-Zhao**[1], **Nicholas Gulati**[13], **Michelle A. Lowes**[13], **Sandra L. King**[1], **Francisco J. Quintana**[5,14], **Young-suk Lee**[10,11], **James G. Krueger**[13], **Kavita Y. Sarin**[12], **Charles H. Yoon**[15,16], **Levi Garraway**[5,6,7,17,18], **Aviv Regev**[5,18,19], **Alex K. Shalek**[5,8,9,20,21], **Olga Troyanskaya**[10,11,22], and **Niroshana Anandasabapathy**[1,23,24,26]

[1]Department of Dermatology, Brigham and Women's Hospital, Harvard Medical School, Boston, MA 02115, USA

[2]Department of Dermatology, Mount Sinai School of Medicine, NY, NY 10029, USA

[3]Department of Genetics and Genomics Sciences Mount Sinai School of Medicine, NY, NY 10029 USA

[4]Population Health Science and Policy, Mount Sinai School of Medicine, NY, NY 10029, USA

[5]Broad Institute of MIT and Harvard, Cambridge, MA 02142, USA

[6]Department of Medical Oncology, Dana-Farber Cancer Institute, Harvard Medical School, Boston, MA 02215, USA

[7]Center for Cancer Precision Medicine, Dana-Farber Cancer Institute, Boston, MA 02215, USA

[8]Institute for Medical Engineering and Science and Department of Chemistry, MIT, Cambridge, MA 02139, USA

[9]Ragon Institute of MIT, Harvard, and MGH, Cambridge, MA 02139, USA

[10]Department of Computer Science, Princeton University, Princeton, NJ 08540, USA

[11]Lewis-Sigler Institute for Integrative Genomics, Princeton University, Princeton, NJ 08540, USA

[12]Department of Dermatology, Stanford University, Stanford, CA 94305, USA

[13]Laboratory for Investigative Dermatology, Rockefeller University. New York, NY 10065, USA

Correspondence to: Niroshana Anandasabapathy.

[25]These authors contributed equally

[26]Lead Contact

Supplemental Information: Supplemental Information includes seven figures, seven tables, and one data file and can be found with this article online at http://dx.doi.org/10.1016/j.cell.2017.06.016.

Author Contributions: Conceptualization: N.A., M.S.-F., O.T., I.T., A.K.S., M.A.L., K.Y.S., C.H.Y. Methodology: N.A., M.S.-F., C.J.N., A.R., O.T., Q.Z., I.T., A.K.S., B.I., R.D., S.P. Software: M.S.-F., R.D., S.P., Q.Z., R.H., D.C., M.R., K.S., I.T., Y.-s.L., A.R., A.K.S. Investigation: C.J.N., Y.L., M.S.-F., S.L.C., S.L.K., J.F.-D., N.G., B.I., S.P., R.D., D.C., T.-G.K., F.J.Q., K.S.P.D., G.X.S.-Z., K.Y.S., N.A. Resources: N.A., F.J.Q., J.G.K., L.G., C.H.Y., M.A.L., A.R. Supervision: N.A., M.S.-F., A.K.S., K.Y.S., O.T., J.G.K. Funding Acquisition: N.A., L.G., A.K.S., A.R., J.G.K., M.S.-F., O.T. Writing: N.A., C.J.N., A.K.S., M.S.-F., R.D.

[14]Department of Neurology, Brigham and Women's Hospital, Boston, MA 02458, USA

[15]Department of Surgical Oncology, Dana-Farber Cancer Institute, Harvard Medical School, Boston, MA 02215, USA

[16]Department of Surgical Oncology, Brigham and Women's Hospital, Boston, MA 02115, USA

[17]Ludwig Center at Harvard, Boston, MA 02215, USA

[18]Howard Hughes Medical Institute, Chevy Chase, MD 20815, USA

[19]Department of Biology and Koch Institute, MIT, Boston, MA 02142, USA

[20]Division of Health Science & Technology, Harvard Medical School, Cambridge, MA 02139, USA

[21]Department of Immunology, Massachusetts General Hospital, Boston, MA 02115, USA

[22]Simons Center for Data Analysis, Simons Foundation, New York, NY 10010, USA

[23]Cancer Immunology and Melanoma, Harvard Cancer Center, Dana Farber Cancer Center, Boston, MA 02215, USA

[24]Harvard Stem Cell Institute, Boston, MA 02115, USA

Summary

Homeostatic programs balance immune protection and self-tolerance. Such mechanisms likely impact autoimmunity and tumor formation, respectively. How homeostasis is maintained and impacts tumor surveillance is unknown. Here, we find that different immune mononuclear phagocytes share a conserved steady-state program during differentiation and entry into healthy tissue. IFNγ is necessary and sufficient to induce this program, revealing a key instructive role. Remarkably, homeostatic and IFNγ-dependent programs enrich across primary human tumors, including melanoma, and stratify survival. Single-cell RNA sequencing (RNA-seq) reveals enrichment of homeostatic modules in monocytes and DCs from human metastatic melanoma. Suppressor-of-cytokine-2 (SOCS2) protein, a conserved program transcript, is expressed by mononuclear phagocytes infiltrating primary melanoma and is induced by IFNγ. SOCS2 limits adaptive anti-tumoral immunity and DC-based priming of T cells in vivo, indicating a critical regulatory role. These findings link immune homeostasis to key determinants of anti-tumoral immunity and escape, revealing co-opting of tissue-specific immune development in the tumor microenvironment.

Graphical abstract

Tumors exploit physiological mechanisms that are in place to keep tissue homeostasis in order to escape the surveillance of the immune system.

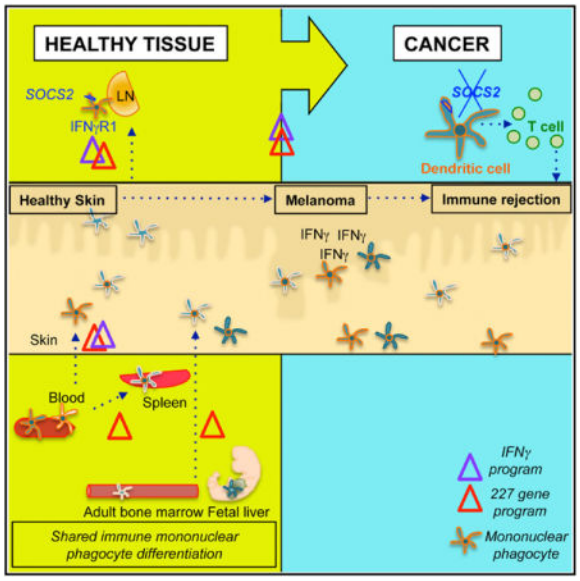

Introduction

The lifetime risk of cancer is linked to the number of stem cell divisions of the corresponding healthy tissue, which physiologically maintain its homeostatic turnover (Tomasetti and Vogel-stein, 2015). Indeed, the majority of human cancers arise in peripheral tissues such as the skin, lung, and colon. Skin cancer prevalence outnumbers all cancers put together (Stern, 2010). However, it is unknown if in tissues with rapid self-antigen turnover such as skin, homeostatic immune programing for the prevention of auto-immunity may impact tumor-immune surveillance. Mechanisms enforcing tissue-specific immunity and those that govern tumor-immune escape remain largely undefined.

Peripheral tissues, blood, and central lymphoid organs (e.g., spleen, lymph nodes [LNs]) are patrolled by immune phagocytes that differentiate from common bone marrow progenitors. These mononuclear phagocytes include dendritic cells (DCs), monocytes, and macrophages. DCs specialize at antigen-presentation of self and foreign antigens. Steady-state DCs surveying tissue continuously migrate (migDC) to draining LNs. DCs present self-antigens released during apoptosis to T cells and direct self-tolerance. However, DCs also initiate immunity to foreign antigens when appropriately licensed by danger signals, such as by pattern recognition receptors (e.g., Toll-like-receptors [TLR]) (Steinman, 2012). In vivo, it is necessary to understand how some DCs maintain tolerance, while others conduct immune priming simultaneously. This is particularly critical at tissue barriers (e.g., skin, lung, and gut), where pathogen encounter is frequent, but where a high rate of self-antigen exposure during UV injury, hair follicle cycling, and epithelial turnover mandates rapid restoration of tissue equilibrium.

Skin migDCs maintain tolerance to self-antigens, despite individual populations having known specialization when licensed to prime during pathogen encounter (Baratin et al., 2015; Waithman et al., 2007). Individual and collective populations of migDCs have also been observed to dampen ongoing immunity to foreign antigens, even in the presence of

TLR adjuvants in vivo (Ananda-sabapathy et al., 2014). Distinct subsets of tissue migDCs share greater transcriptome relatedness with each other than they share with functional counterparts that reside in central immune organs (e.g., LN cDCs) (Anandasabapathy et al., 2014; Miller et al., 2012). These findings suggest that a common differentiation program is conferred in peripheral tissues, which regulates tissue DC function. It is important to understand how shared programming occurs in healthy tissue and impacts barrier surveillance to pathogens and detection of malignant self-transformation that occurs during early cancer progression.

We previously identified a 227 gene program shared by skin-derived DC subsets in the steady state and conserved across humans and mice. This program centers on NFκβ signaling and is enriched for many tolerance-related genes such as the receptor programmed death ligand 1 (PD-L1), immunosuppressive indo-leamine 2,3-dioxygenase (IDO), and CD200 (Anandasabapathy et al., 2014). Mice with a DC-specific deficiency in the NFκβ sub-unit Iκκβ fail to accumulate tissue-derived migDCs in the draining LNs and develop spontaneous autoimmune lupus-like disease (Baratin et al., 2015). Collectively, these findings link NFκβ–dependent differentiation of migratory DCs to protection from autoimmunity and tissue homeostasis. These data support a regulatory role for these populations and this program in peripheral self-tolerance. It is unknown how this program is conferred, how homeostasis is mediated, and whether it can be used to identify key determinants of tumor-immune surveillance.

To address these questions, the present study interrogated if and how this program is enforced in peripheral tissue. We find that, despite functional specialization, differentiated subsets of DCs, monocytes, and macrophages share enrichment of these 227 transcripts at multiple stages of progenitor differentiation, tissue entry, and migration. This program is conserved in fetal and adult development and across species. IFNγ signaling impacts antigen processing and presentation pathways in DCs migrating from skin and conditions a majority of these transcripts, revealing a critical instructive role. Remarkably, we find that IFNγ-dependent programming and 227 transcripts enrich and correlate across multiple human cancers of tissue. 227 modules are expressed in DCs and monocytes isolated from human metastatic melanoma and relate to IFNγ-dependent programing on a per-cell and -population basis. Both programs are strikingly induced in primary cutaneous human melanoma as compared to abnormal moles, common moles, or healthy skin and stratify metastatic melanoma survival. We use this program to identify a single highly enriched and developmentally conserved transcript within the 227 signature, *suppressor-of-cytokine-signaling 2* (*SOCS2*). SOCS2 is expressed in tissue migratory DCs, but not LN resident DCs in mouse, and in human $CD11c^{+}$ mononuclear phagocytes infiltrating primary melanoma. SOCS2 loss enables robust immune-mediated tumor rejection, and SOCS2 has a key in vivo regulatory role in DCs. These findings link immune homeostasis in tissue to programing in tumor. IFNγ conditions a shared differentiation program among mononuclear phagocytes in peripheral tissue, which is coopted during tumor growth and which can be used to identify critical molecular determinants supporting adaptive immune resistance.

Results

Shared Lineage, Species, and Developmental Conservation of a Homeostatic Differentiation Program across Mononuclear Phagocytes in Tissue

First, to assess if species-conserved transcripts favoring tissue homeostasis are shared by other tissue mononuclear phagocytes, as might be expected from micro-environmental conditioning, we compared expression analysis of the 227 gene homeostatic signature in different lineages of human mononuclear phagocytes in skin and blood (Figures 1A and S1A). We observed that human skin-resident DCs and monocyte-derived-macrophages (GEO: GSE35459 [Haniffa et al., 2012; McGovern et al., 2014]) share induction of 227 core signature genes when compared to blood counterparts, indicating conservation across monocyte and DC lineages in peripheral tissue (Figure 1A). To determine if such induction is specific for tissue entry, we simultaneously examined 227-signature expression at multiple developmental transitions in parallel. Second, we tested signature induction during mononuclear phagocyte egress from the skin to the LN by comparing expression of signature genes in DCs and monocytes directly isolated from skin to those that migrated from skin to draining LN (GEO: GSE49358) (Tamoutounour et al., 2013) (Figure 1B). Third, we included a comparison of the same signatures from LN-resident classical DCs (cDCs) derived from blood-born precursors against those migDC subsets in LN that have migrated from skin (and from which the original signature was defined [GEO: GSE53588]) (Anandasabapathy et al., 2014) (Figure 1C). Fourth, we compared blood-derived DC progenitor subsets (pre-DC) to differentiated classical cDC counterparts in spleen—a central lymphoid tissue (GEO: GSE60782) (Schlitzer et al., 2015) (Figure 1D). Fifth, we tested monocyte and macrophage progenitors, and their differentiated subsets isolated from adult blood or fetal liver, against those isolated directly from embryonic fetal skin (GEO: GSE66970) (Hoeffel et al., 2015) (Figure 1E). A statistically significant change in the major portion of signature genes (76%–93%) was observed at each defined transition (Figures 1A–1E, gated groups [red versus blue]) in either progenitor differentiation or tissue entry (represented as triangles, Figures 1F and S1A–S1C and Tables S1A and S1B). Thus, 227 homeostatic signature genes are species-conserved (mouse and human), lineage-conserved across individual subsets of mononuclear phagocytes (DC, monocytes, macrophages), and developmentally conserved (sharing fetal and adult differentiation in tissue). Conserved signatures enrich upon differentiation in central lymphoid or peripheral tissue and upon migration into or from peripheral tissue.

IFNγ Is a Sufficient Instructive Cue for Homeostatic Programming in Human Mononuclear Phagocytes and Tissue

To identify conditioning cues for this program, we conducted over-representation analysis and gene set enrichment analysis (GSEA) (Table S2A and data not shown). The developmental signature we identified overlaps with genes related to early TLR activation by LPS-triggered NFκB activation (Dalod et al., 2014). We also noted high correlation to hallmark programs of TNFα signaling through NFkB, IL-2Stat5, and with IFNγ hallmark genes (MSigDB's hallmark collection). These programs share many points of convergence. LPS triggers transient early IFNγ release (Frucht et al., 2001), LPS and IFNγ synergistically act via Stat1, and TNF and IFNγ signaling share common targets (Schroder et al., 2004).

Prior work revealed that MyD88$^{-/-}$ X Trif$^{-/-}$ mice, germ-free mice, and TNFSFR1$^{-/-}$TNFSFR2$^{-/-}$ mice have no defect in DC migration, as a measure of differentiation (Baratin et al., 2015) (Wilson et al., 2008). These data suggest that TNFα, IL-1, and LPS may be compensated by other cues. Therefore, we extended our analyses to a collection comprised of over 200 gene sets specifically related to human skin populations, human immune cells, and skin diseases (Table S2A).

Using this collection, we observed that 227 signature genes statistically associate with transcripts induced in monocyte-derived macrophages derived from human patient peripheral blood mononuclear cells 24 hr after culture with either low dose IFNγ (20 ng/mL, adjusted p = 5.67×10^{-21}) or with IFNγ + LPS (adjusted p = 9.67×10^{-25}). Importantly, this signature was not associated with human monocyte-derived macrophages cultured with media alone or with other cytokine treatments at 24 hr, such as TNFα, LPS, IL-4, and IL-17 (Figure 2A and Tables S2A and S2B, GEO: GSE18686 [Fuentes-Duculan et al., 2010]). Induction of 227 genes was also identified in whole-skin biopsies taken from 10 healthy or 10 psoriatic individuals 24 hr after IFNγ was injected into their skin, when compared against paired placebo or control biopsies from the same individual (adjusted p = 2.16×10^{-15}) (Figure 2B and Table S3A). These data indicate IFNγ is sufficient to condition a large fraction (68%– 75%) of 227 gene signatures in cultured human mononuclear phagocytes or when injected directly into the skin of human subjects.

We then examined relatedness of transcripts enriched during differentiation to those following IFNγ induction by cross-comparison of these seven datasets (Figure 2C). We performed analysis both within the 227 gene signature set and across all available transcripts for comparison across platforms. We noted higher Pearson correlation (r) within the 227 signature genes (Figure 2C left versus right). Higher correlation was seen between transcripts changed (log2FCH) during skin migration (sets A, B, and C), skin entry (sets A and E), and progenitor differentiation (sets D and E). As expected, sets including treatment with IFNγ in vitro and in vivo were correlated within the 227 signatures (r = 0.38) and across all transcripts (r = 0.43). Intriguingly, we also observed that within the 227 program, genes differentially expressed between human skin and blood mononuclear phagocytes correlated with those induced in IFNγ-treated human mononuclear phagocytes (sets A and F, r = 0.49, Figure 2C). To further probe this association, we derived an IFNγ transcrip-tome signature. 1,217 IFNγ-dependent up and 1,210 IFNγ downregulated transcripts were identified by comparing human mononuclear phagocytes treated with IFNγ and IFNγ plus LPS against all non-IFNγ treatments (untreated controls, TNF-α, IL-4, LPS, and IL-17, GEO: GSE18686). As positive and negative control groups for validation, we applied these IFNγ-induced signatures (or an equal number of random probes) to the dataset from which it was derived (GEO: GSE18686, Figures S2A and S2B). For individual samples, the overall expression of each 227- or IFNγ-specific up and downregulated signature was summarized using Z scores and compared in parallel. We noted a marked positive and negative enrichment in IFNγ-dependent (IFNγ-signature) up (orange bars) and downregulated transcripts (purple bars), respectively, while comparing individual subsets of human skin mononuclear phagocytes against those in blood (Figure 2D). This trend was visible across all developmental transitions analyzed and when applied to IFNγ-injected patient skin

specimens (Figures S1C and S2C). These data suggest that IFNγ-induced transcripts and those induced during mononuclear phagocyte differentiation are largely shared.

IFNγR1 Signaling Is Necessary for Homeostatic Differentiation of migDC

To test if IFNγ is not only sufficient but also necessary to condition DC, we compared the transcriptome of migDC isolated from skin draining LNs of IFNγR1$^{-/-}$, wild-type (WT), and IL27Rα$^{-/-}$ mice. IL-27Rα mice were included as a control for IFNγ receptor specificity. IL27Rα signals through Stat3 and Stat1 and has a known role in suppressing DC activity and autoimmune inflammation (Mascanfroni et al., 2013). Little difference was appreciated between the transcriptome of steady-state migDC isolated from IL27Rα$^{-/-}$ and C57BL/6 WT mice, suggesting little basal signaling through IL-27Rα. In contrast, migDC from IFNγR1$^{-/-}$ mice differed from WT migDC in 277 differentially expressed transcripts (S2D, Table S3B, FDR < .2, FC > 1.5, n = 3 individual mice). These included transcripts known to condition DC development such as Flt3, RelB, and Stat5b (Figure S2D), to relate to antigen processing and MHCI loading (e.g., TAPBP, TAP1), to regulate proteasome activity, and to associate with autoimmunity and inflammation (PSMB8, PSMB3) (Tables S3C and S3D). By ingenuity pathway analysis (IPA), significant pathways identified included death receptor signaling, DC-NK cross talk, interferon signaling, apoptosis, antigen processing, and GM-CSF signaling (Figure S2E), and top networks included antigen presentation ($p < .01$, Figures S2E and S2F). We then tested if IFNGR1$^{-/-}$ migDC were deficient in the 227 differentiation or IFNγ-dependent programs. To do this, we used GSEA to test if a given signature tends to cluster at the top of the most (up or down) regulated genes (Table S3E). 227 and IFNγ signatures were among the most significant downregulated genes in IFNGR1$^{-/-}$ versus WT comparisons. We also tested loss of IFNγ and 227 signatures in IFNGR1$^{-/-}$ migDC by using gene set variation analysis (GSVA). We observed concordant loss of 227 (Figure 2E) and IFNγ-dependent upregulated signatures (Figure 2F GSVA, IFNγR1$^{-/-}$ versus WT, 227 up FDR adjusted p value < .01; IFNγR1$^{-/-}$ versus WT, IFNγ up, FDR adjusted p value = 0.09), leading to an overall significant difference in total IFNγ and 227 signatures (GSVA, IFNγR1$^{-/-}$ versus WT: total IFNγ, FDR adjusted p value < .05; IFNγR1$^{-/-}$ versus WT: total 227 FDR adjusted p value < .01, Table S3F). Correlated GSVA scores were observed across samples in the upregulated portion of both signatures (e.g., r = 0.91, CI = [0.63-0.98]), but not the downregulated transcripts (r = 0.74, CI = [0.15-0.94]). Collectively, these data indicate that IFNγ is both necessary and sufficient to induce 227 upregulated signature transcripts.

IFNγ-Dependent and 227 Homeostatic Signatures Enrich and Correlate across Multiple Human Primary Cancers and Stratify Metastatic Melanoma Survival

To test the relevance of these findings in clinical disease sets, we conducted a search-based exploration of expression compendia analysis (SEEK) of human datasets across the Gene Expression Omnibus and Cancer Genome Atlas (TCGA) (Zhu et al., 2015) (Figure 3A). The 227 signature had markedly higher co-expression scores (i.e., dataset weight) across the SEEK compendia as compared to random queries of matched size, with such scores highly significant (at $p \leq 0.001$) in over 87% of the datasets. Surprisingly, when the top 200 sets were examined, a large number of top sets were associated with cancer (57/200 top datasets,

p = 7.99e-13, Figure 3A and Table S4), in addition to expected sets of DCs and mononuclear phagocytes (8/200 top datasets, p = 4.37e-3, Table S5).

In cancer, IFNγ drives immunosuppressive IDO and PD-L1 expression (Harden et al., 2011; Taube et al., 2015), two transcripts within the 227 signature. To further interrogate if IFNγ and 227 signatures were enriched in primary human cancers and correlate, we compared the top 150 IFNγ transcripts (sorted by false discovery rate), the top 200 homeostatic signatures, or 200 random probes and tested expression across a range of cancers. Both IFNγ signatures and homeostatic programming genes were observed to enrich across a range of primary human tumors almost exclusively of peripheral tissues, including melanoma skin cancer (Figures 3B and S3A). Within these primary specimens, a strong correlation was noted between those tumors bearing the 227 signatures and IFNγ signature expression (Pearson correlation:0.5-1; Figure 3B bar). In contrast, primary tumor samples with high or low expression of IFNγ, or of 227 signatures, did not overtly relate to total somatic gene level mutations or copy number variance (Figures S3B– S3G). These data suggest that tissue programing is closely associated to IFNγ in the tumor microenvironment. Also, in patients with metastatic melanoma, expression of high, medium, or low levels of either the 227- or the IFNγ-induced signatures is associated with high, medium, and low survival (Figures 3C and 3D). A low somatic mutation rate portends poor long-term survival, whereas those with a medium or high somatic mutation rate portend high and intermediate long-term survival, respectively, using the same data (Figure 3E). Samples stratified as having high, medium, or low 150 IFNγ signatures largely co-correlated with those having high, medium, or low 227 signatures but were distinct from those bearing a high, medium, or low somatic mutation rate (total non-silent missense and nonsense mutations [Figures 3F and S3B–S3G]). These findings indicate that in patients with metastatic melanoma, increased expression of IFNγ-related inflammation and mononuclear phagocyte immune signatures is associated with improved long-term clinical outcomes.

Single-Cell Transcriptome Profiling of Human Melanoma Metastases Suggests Enrichment of the Homeostatic Differentiation Signature in DCs

To further investigate the relationship between the IFNγ- and 227-gene signatures and to test enrichment in tumor-associated mononuclear phagocytes, we performed single-cell transcriptome analysis of 333 individual DCs and monocytes sorted from a single LN melanoma metastasis (Table S6, comparison of this study to prior studies by Tirosh et al., 2016; Patel et al., 2014). To isolate these cells, we used an enrichment strategy for lineage negative (lineage: CD3/CD20/CD56/ CD66b) $CD45^+CD11c^+HLA^+$ cells, distinguishing $CD14^+$ cells as enriched for monocytes from $BDCA1^+$ and $BDCA3^+$ expressing populations by flow cytometry. Transcriptional analysis of $BDCA3^+$ enriched cells revealed two distinct subpopulations (Figures 4A and S4A): one closely related to $BDCA3^+$ classical, myeloid DCs, and the other to published reports of plasmacytoid DCs (PDCs) that express high levels of CD123 transcripts (Figure S4B and Table S7A). We compared sequences from these BDCA1 cDC, $BDCA3^+$ cDC, $BDCA3^+$ $CD123^+$ cells, and monocytes to those previously described across other cell types (cancer associated fibroblasts [CAFS]; melanoma cells, T, B, and natural killer (NK) cells; endothelial cells; and macrophages) (Tirosh et al., 2016). A subset of genes from both of the 227 up and downregulated modules (Figure 4B) was

regulated among mononuclear phagocytes. We also observed that the 227 genes normally downregulated in tissue DCs (227 down) were enriched in tumor-resident DCs. This list of genes includes transcripts related to DC activation and cross-presentation of dying cells by DCs, which include Clec9A, Batf3, and WAS, as well as cellular processes such as autophagy (e.g., RAB32).

To look for evidence suggesting that IFNγ could enforce the 227-gene program in the tumor microenvironment, we next tested if IFNγ- and 227-gene signatures correlated with each other (Spearman correlation). We found that, within an individual cell in a given population, a single cell's 227 and IFNγ signatures were significantly positively correlated ($r > 0.3$ and 0.44; up and down respectively; p value < 0.001, paired t test; Figures 4C and S4C; calculation described in STAR Methods). To test the correlation of the 227 and IFNγ signatures between populations, we generated 100 in silico bulk signatures from 40 random subsets of cells from each population and calculated the correlation between the 227 and IFNγ signatures (Figure 4D and S4D). This analysis revealed that intra-population correlation was always higher than inter-population correlation for every population in both the up and down components of each signature (p value < 0.003 and 0.00005;up and down respectively; Welch's t test, Tables S7B–S7E).

IFNγ-Programming and Tissue Mononuclear Phagocyte Signatures, Including SOCS2, Are Associated with Primary Cutaneous Melanoma

One pathway by which melanoma skin cancer is thought to arise is from the increased malignant transformation potential of nevi or moles (Elder, 2016) and from UV injury of healthy skin. To compare levels of 227- and IFNγ-signature induction in cancer against normal skin and nevi, we tested the relative level of IFNγ signatures and 227 homeostatic transcripts present in microarray analysis of normal human skin, common nevi (low malignant potential), dysplastic nevi (high malignant potential), and primary cutaneous melanomas taken by diagnostic patient biopsy. We observed a graded increased enrichment in both the IFNγ- and 227-gene signatures (*Z* score), with marked enrichment in primary cutaneous melanoma (Figures 5A and S5A). Positive enrichment of both 227- and IFNγ-signature up and downregulated transcripts was observed in melanoma (Figures 5A, 5B, and S5A) and occurred irrespective of directionality (Figures S5B and S5C). These data indicate that IFNγ and 227 signatures closely associate with human primary cutaneous melanoma.

We reasoned that this program might help us identify key determinants of tumor-immune surveillance. Developmental genes likely to encode critical regulators of the adaptive immune response to cancer would be (1) highly expressed during mononuclear phagocyte differentiation in tissues, (2) induced by IFNγ in human skin and in monocytes, and (3) present in melanoma when compared to normal skin. Within the 227 genes, we identified 37 transcripts that intersect those present across all 5 developmental sets (n = 97) that are induced during IFNγ conditioning in vitro (n = 154) and in vivo in human subjects (n = 131) (Figure 5C, left). Half of all 227 transcripts (n = 113) were enriched in primary cutaneous melanoma relative to normal skin (FDR < 0.05). Among the 20 transcripts converging in development, induced by IFNγ in vitro and in vivo, and enriched in primary melanoma (Figure 5C, right), *SOCS2* was notable as one of the most highly differentially expressed

transcripts (> 30-fold enriched) across tissue DCs in both human and mouse species when compared to LN resident or blood counterparts (Anandasabapathy et al., 2014).

SOCS2 is a member of the SOCS family of cytokine-induced Jak-Stat regulators and is uniquely able to degrade all other family members (Greenhalgh et al., 2005; Rico-Bautista et al., 2006). *SOCS2* transcripts were enriched in all developmental transitions into or from tissue (Figure 5D), and SOCS2 protein is expressed in skin-derived migDC, but not in LN-resident CD8a cDC (Figure 5E). In IFNγR1$^{-/-}$ as compared against IFNγR1$^{+/+}$ migDC, *SOCS2* transcripts were ~4 times lower expressed (FC = 3.92, p = 0.0062, FDR = 0.28, Table S3D), suggesting possible IFNγ dependence under steady-state conditioning. We also noted that SOCS2 protein was expressed after IFNγ conditioning of Flt3L-dependent classical DC, derived by bone marrow culture (Figure 5F).

To test if SOCS2 is expressed in mononuclear phagocytes in the tumor microenvironment, we co-stained SOCS2 and CD11c in frozen sections from common nevi, dysplastic nevi, and primary cutaneous melanoma of the same skin biopsy specimens we previously analyzed by microarray (n = 5–7 patients specimens per condition). Strikingly we observed an increasing infiltrate of CD11c^{+} cells of a mononuclear phagocytic morphology bearing numerous dendrites, located within involved regions of dysplastic nevi and primary cutaneous melanoma specimens, which co-stained for SOCS2 (Figure 5G). SOCS2 expression was detected in cells bearing a dendritic morphology across multiple primary cutaneous melanoma patient specimens (Data S1). Enrichment of *SOCS2* transcripts also correlated with basal cell skin cancer subtypes ranked by aggressiveness (Figure S5D). These data indicate that SOCS2 is induced by IFNγ and is present on mononuclear phagocytes infiltrating the tumor microenvironment of early primary human cutaneous melanoma as part of a tissue signature induced during early human melanoma formation.

SOCS2 Inhibits Tumor-Immune Rejection

To investigate if SOCS2 contributes to peripheral immune surveillance to cancer, we compared intradermal tumor growth in *SOCS2*$^{-/-}$ and control mice. *SOCS2*$^{-/-}$ mice had no overt defects in immune cell numbers consistent with prior reports (Figures S6A–S6D). EL4-OVA thymoma is an immunogenic model of cancer growth in which antigen-specific immunity can be assayed. *SOCS2*$^{-/-}$, but not *SOCS2*$^{+/+}$, mice had a 70%–90% reduction in intradermal EL4-OVA growth, with regression starting around day 8–12. We noted higher levels of IFNγ production by antigen-specific CD8 T cells isolated from the LNs and spleen of *SOCS2*$^{-/-}$ animals upon peptide re-challenge, suggesting that immune-mediated mechanisms support tumor rejection (Figure 6A). Testing B16-OVA melanoma, we also observed a roughly 40% reduction of intradermal tumor growth in *SOCS2*$^{-/-}$ animals (Figure S6E). To test DC-specific acute SOCS2 loss, we used mixed-bone-marrow chimerization and diphtheria toxin ablation. Mice with a transient restriction to *SOCS2*$^{-/-}$ ZBTB46-dependent DC at the time of tumor implantation (Figure 6B and 6C) showed a significant reduction in B16-OVA melanoma growth. Higher CD8/T_{reg} ratios were observed in tumor-infiltrating lymphocytes (TILs), suggesting that tumor rejection was immune mediated (Figure 6C). Upon further therapeutic anti-tumor priming by vaccinia-OVA scarification after B16-OVA implantation, mice with uncompensated loss of *SOCS2* in

ZBTB46-dependent DC demonstrated smaller viral lesion diameter and also demonstrated higher IFNγ production when polyclonal $CD8^+$ T cells were isolated directly from TILs and recalled with OVA-specific peptides (Figure 6D). Likely due to the efficiency by which vaccinia-OVA immunization is protective, no significant further improvement in tumor protection was noted overall. Thus, SOCS2, as part of a highly enriched core homeostatic signature, suppresses peripheral tumor immune surveillance by DCs.

SOCS2 Dampens In Vivo Adaptive Immune Priming by DC-Autonomous Mechanisms

To further interrogate DC-specific SOCS2 activity during T cell priming, we tested SOCS2 activity using a DC-dependent protein-immunization model. Anti-CD205 antibodies deliver the HIV gagp24 antigen to the C-type lectin CD205 on the surface of DCs (αCD205-gagp24), allowing efficient endosomal targeting and antigen presentation. Protein immunization was administered with a TLR adjuvant to direct DCs to priming (Bonifaz et al., 2004). In this model, immune priming directly depends on classical DC, whereas migDC have known suppressive activity (Anandasabapathy et al., 2014). *SOCS2*$^{-/-}$ mice had higher ex vivo antigen-specific CD4 effector responses to immunization as measured by CD4 p24-specific IFNγ production (Figures 7A– 7C). These data indicate that SOCS2 limits immune priming of T effectors during DC-based immunization. We observed expanded immunity without a loss of $CD4^+$ T regulatory cell (T_{reg}) numbers in the spleen or dLN (Figures S7A and S7B). In addition to constitutive loss during DC-dependent priming, we tested acute uncompensated loss of *SOCS2* in the DC compartment at the time of immune priming by mixed bone marrow chimerization. In the presence (but not absence) of diphtheria toxin (DT), restricted *SOCS2* loss to DCs just prior to prime and boost recapitulated the phenotype of global *SOCS2* loss and expanded T effector activity (Figures 7D and 7E) and proliferation (Figure S7C). This suggests that intrinsic SOCS2 activity in DCs is sufficient to mediate immune dampening of T cells. Higher polyfunctional T cell activity was also observed (Figure 7F). T cell intrinsic SOCS2 activity did not contribute to dampening adaptive T cell immunity, as adoptive transfer of *SOCS2*$^{-/-}$ or WT T cells to Rag2$^{-/-}$ recipients did not impact priming (Figures 7G and S7D). Taken together, these data reveal that SOCS2 activity in DC is sufficient to significantly limit adaptive T cell immunity in vivo. To further confirm that SOCS2 activity in DC-based adaptive immune priming was not model specific, we also tested SOCS2 activity during contact sensitization (delayed type hypersensitivity response), which, unlike DC-targeted protein immunization, depends on $CCR7^+$ skin migDC to transport antigens (Ohl et al., 2004). CCR7-restricted loss of *SOCS2* led to significantly higher contact sensitization as measured by ear swelling (Figure 7H). Thus, SOCS2, a highly enriched species-conserved factor specified during homeostatic programming, directs adaptive immune tolerance during DC-based priming.

Discussion

Immune homeostasis requires rapid initiation and control of an immune response. We find that all tissue mononuclear phagocytes share core regulatory genes associated with tissue homeostasis and differentiation, across species, and across development. Such a program may provide an evolutionary conserved mechanism to balance protection to pathogen challenge with immune regulation. Induction of a conserved differentiation gradient across

blood, tissue, and lymphoid organs may help to spatiotemporally segregate activity of DCs in compartments (e.g., LN derived and skin migratory) and contribute to coordinated priming and tolerance during an ongoing immune response in vivo. As an example, an increase in signature genes like Fas might promote apoptosis, which prevents autoimmunity by limiting available antigen to T cells (Kushwah and Hu, 2010). Defects in DC apoptosis are linked to autoimmune disease (Chen et al., 2006). The uptake and antigen transfer of apoptotic cell fragments by rapidly dying migratory cells has been suggested to induce peripheral T cell tolerance (Inaba et al., 1998).

We find IFNγ to be sufficient to induce 227 transcripts and observe an uncompensated loss of IFNγ signatures normally up-regulated during differentiation in IFNγR1$^{-/-}$ migDC. These data reveal that IFNγ is an instructive cue in steady-state mononuclear phagocyte differentiation. In the absence of IFNGR1, migDCs have changes in death receptor signaling, apoptotic pathways, and antigen processing (FigS2E). Interrogating these processes in the presence and absence of IFNGR1 signaling in vivo is needed. During early skin cancer formation, the immune system must distinguish abnormally transformed pre-cancerous cells from the turnover of healthy cells in tissue. Lifetime risk of cancer in a particular tissue is linked to the number of divisions of normal self-renewing cells that maintain its homeostatic turnover (Tomasetti and Vogelstein, 2015). This might be extended to consider the impact of homeostatic turnover on immune programming and development. A transcriptional program coupling tissue-immune surveillance to regulation by apoptotic death may be appropriate in healthy tissue but could leave a blind spot to tumors of peripheral tissues with a high mitotic rate. Therefore, relating these signatures to the proliferation of surrounding cells and the uptake of dying cells would be an important future direction.

IFNγ-signature scores change during multiple developmental transitions. These include tissue entry and progenitor differentiation, suggesting a pervasive role (FigS2C). Further study will test if and how IFNγ functions as a local conditioning cue. As an alternative to tissue-based conditioning, mononuclear phagocytes could be pre-emptively differentiated by IFNγ during bone marrow development, which is differentially halted or enforced in a tissue-specific manner. In line with this, during acute toxoplasma infection, bone marrow NK-based production of IFNγ conditions monocytes toward tolerogenic function through CD200 (Askenase et al., 2015), a hallmark gene present within the 227 signature. Because we detect an uncompensated loss of IFNγ up signatures in IFNGR1$^{-/-}$ mice, the role of STAT1 and IRF1 tonic transcriptional regulation will be considered independently from other cues, which may independently regulate the downregulated module. Indeed, while genes related to DC cross-presentation, licensing by death receptors, and activation (e.g., BATF3, XCR1, CLEC9A, WAS, and CD36) are downregulated during homeostatic differentiation in tissue, we find that 227 and IFNγ modules that are downregulated in DCs in tissue are increased instead in primary melanoma, as compared to skin and nevi. This suggests that there is potential for an uncoupled regulation of the up and down modules, which could be exploited for therapeutic benefit. Also, although we did not identify a correlation between IFNγ signature induction and non-silent gene mutations in metastatic melanoma, key antigenic mutations and epitopes, rather than the overall mutational burden,

might be more relevant to directing the level of T-cell-specific immunity, as was suggested in the response to immune checkpoint blockade (Snyder et al., 2014), and will be tested.

When comparing healthy tissue to primary cancer, levels of IFNγ and 227-gene signature modules are strikingly higher in primary cutaneous melanoma than in skin or nevi. IFNγ-dependent and 227-gene signatures closely co-correlate to each other and positively stratify melanoma survival, likely as indicative of an anti-tumoral immune response. Therefore, these signatures may have utility as biomarkers. Future studies testing programmatic change during tissue development and acute versus chronic inflammation in the tumor setting will likely reveal a dynamic modulation of myeloid differentiation and activity. Such immune modulation in DCs may confer greater CD40 and IL-12 dependence, altered DC-NK cross talk (such as by IL15R), or mediate differences in early and late activity such as by delayed induction of immunosuppressive IDO (Harden et al., 2011). Homeostasis encompasses not only immunosuppressive, tolerogenic molecules CD200, IDO, PDL1, and SOCS2, but also those that are immunostimulatory (CD40). CD40 regulates DC activation, cytokine production, and non-canonical NF-κB signaling (Ma and Clark, 2009). Hence, further work is needed to understand the overall balanced regulation of mononuclear phagocyte activity by this program and the functional outcomes from such a balance, for example, testing antigen presentation function in the setting of tumor. IFNγ-dependent DC differentiation may tune type I IFN signaling, and IFNGR1$^{-/-}$ migDCs were observed to have differences in IFN signaling transcripts (Figure S2E).

While adaptive immune editing and anti-tumoral immunity are IFNγ dependent (Dunn et al., 2006) (Kaplan et al., 1998), IFNγ is not singularly beneficial in clinical use, which may speak to cell-type-specific differences. In melanoma patients, despite the predicted success of IFNγ, and in contrast to Type 1 IFNs (IFNα/β), IFNγ treatment was associated with T cell suppression and worsened clinical outcomes (Mellor and Munn, 2008; Zaidi and Merlino, 2011). Production of IFNγ by T and NK cells infiltrating tumors is necessary for cytotoxic activity but may provide micro-environmental conditioning that recapitulates homeostatic differentiation in the myeloid compartment, promoting self-tolerance. In line with this, T cell production of IFNγ induces local PD-L1 and IDO expression in tumors.

IFNγ-dependent and 227-gene programming co-enrich not only in melanoma, but also across multiple human cancers. These findings suggest that IFNγ instructs anti-tumor immunity by recall of this differentiation program broadly. Developmental co-opting in the tumor microenvironment might direct adaptive immune resistance by inducing key immunosuppressive transcripts that are permissive to tumor-immune evasion. Hence, loss of *SOCS2*, a species-conserved transcript highly expressed by tissue migratory DC that was recently linked to suppression of autoimmunity (Rothhammer et al., 2016; Yeste et al., 2016), enables robust tumor-immune rejection. SOCS2 loss liberates anti-tumoral immunity by expanding DC-based T cell priming and antigen-specific adaptive immunity. These data link adaptive immune resistance to immune development in tissues and suggest that failed immune rejection of tumors may occur as a consequence of highly conserved programmatic mechanisms preserving tissue immune homeostasis.

Contact For Reagent and Resource Sharing

Further information and requests for resources and reagents should be directed to and will be fulfilled by the Lead Contact, Niroshana Anandasabapathy (nanandasabapathy@partners.org).

Experimental Model and Subject Details

Mice

6-8 week old female mice were bred and/or housed in a specific pathogen free facility at Harvard University. For biochemistry analyses alone, both female and male mice were chosen. All experiments involving laboratory animals were performed under protocols approved by the Harvard Medical Area Standing Committee on Animals (Boston, MA) and the Harvard University Animal Care and Use Committee approved all protocols. C57BL/6N mice (WT), CD45.1^{+}, and CCR7$^{-/-}$ mice were purchased from Taconic or Jackson Labs to pair to the genotype of the experimental strain in use. Zbtb46-DTR mice were originally provided by Michel Nussenzweig and bred for an additional 6 generations or more within our facility. SOCS2$^{-/-}$ mice were originally created on a C57/Bl6 background and generously provided by Drs. Doug Hilton and Warren Alexander. All mice were used at 6-10 weeks of age and were age and gender matched for each experiment.

T cell Reconstitution

For T cell reconstitution experiments, CD3^{+} T cells were isolated by magnetic bead depletion using a biotinylated cocktail of antibodies against CD11b, Ter119, B220, Gr1, DX5, and IAIE, followed by negative selection with anti-biotin microbeads (Miltenyi). Rag2$^{-/-}$ mice received 1.5-2×10^{6} WT or SOCS2$^{-/-}$ T cells, and were allowed to reconstitute for 12 weeks prior to use.

Mixed Bone Marrow Chimeras

For BM chimeras, 8-week-old recipients were irradiated (500 cGy plus 550 cGy with 3h rest between irradiation sessions) prior to intravenous reconstitution with 1.5×10^{6} WTor SOCS2$^{-/-}$ BM cells mixed with 1.5×10^{6} ZBTB46-DTR or CCR7$^{-/-}$ BM cells by intravenous injection. Mice were maintained after radiation on antibiotic supplemented water (Sulfatrim) for 12 weeks prior to use.

Murine Tumor Implantation

B16-OVA were obtained from the laboratory of Arlene Sharpe and EL4-OVA cells were obtained from the laboratory of Charles Drake. 2×10^{5} cells were implanted intradermally in C57BL/6J or SOCS2$^{-/-}$ host mice (Day 0), and tumor growth was monitored over time using digital calipers and the modified tumor growth formula, or 0.5(L×W^{2}). For experiments utilizing BM chimeric mice, 1×10^{6} B16-OVA was implanted intradermally, and 1 μg DT was administered on day 0 and Day 1, while 0.5 μg DT was administered on Day 3, 5, and 7.

TILs Isolation

For isolation of tumor-infiltrating lymphocytes (TILs), tumors were carefully excised. Tumors were mechanically disrupted, washed in 40mL of 1× PBS, 2-4 times and filtered through a 70 μM filter prior to enrichment of lymphocytes using density gradient centrifugation with Percoll (GE Healthcare). Stock solutions were prepared by combining 90% Percoll and 10% HBSS (10×) to produce a working solution. Using the working solution, 40% and 80% solutions were produced. Tumor pellets were washed in a volume of 50 mL PBS, resuspended in the 80% Percoll solution, and layered beneath the 40% Percoll solution. This gradient was spun at 2,000 RPM for 20 min, with no brake, at room temperature. A cell layer at the density interface was collected and thoroughly rinsed in 50 mL PBS, and then stained. For calculation of the CD8/Treg ratio, total numbers of $CD8^+$ and $CD4^+CD25^+FoxP3^+$ were calculated by multiplying the counted totals of TILs by the frequency of the individual cell types.

Vaccination Protocol

Protein vaccinations and recall assays were performed as previously described (Anandasabapathy et al., 2014). Briefly, age and gender-matched control and experimental mice were injected subcutaneously in the footpad with 0.5 μg αCD205-gag p24 with 20 μg of GLA-SE (Immune Design Research Institute). Identical boost vaccination was administered exactly 4 weeks later. One week following boost vaccination, spleen and peripheral LN cells were analyzed for effector cytokine production by 6 hr intracellular staining as well as CFSE 4 day cultures. In experiments utilizing mixed bone marrow chimeras and diphtheria toxin (DT), 0.5 μg DT was administered on day-3 and day-1 prior to both the prime and boost doses.

Contact Hypersensitivity

Contact hypersensitivity experiments were performed as previously described (Martin, 2013). Briefly, mice were anesthetized by i.p. injection of ketamine, and a patch of dorsal hair was removed using an electric shaver. For sensitization, 20 μL of 0.5% dinitrofluorobenzene (DNFB; Sigma D1529) in acetone/olive oil (AOO) at 4:1 ratio was painted on the shaved dorsal skin on day 0 and day 1. For elicitation, 10 μL of 0.2% DNFB in AOO was painted on each side of one ear on day 5, while 10 μL of AOO only was painted on each side of the other ear as a control. Measurement of ear thickness was performed right before elicitation and every 24h afterward using a thickness gauge.

Methods Details

Cell Lines

B16-OVA and EL-4 OVA cells were provided by Drs. Charles Drake and Arlene Sharpe. All cell lines were grown in DMEM (GIBCO) with 10% FCS (GIBCO and Gemini) and Penicillin/Streptomycin (GIBCO)for no more than 3 passages prior to implantation and tested free of mycoplasma using the MycoScope PCR Mycoplasma Detection kit (Genlantis, San Diego, CA), according to the manufacture's instructions.

Virus Preparation and Vaccinia scarification

VACV-OVA was provided from Jonathon Yewdell, and was expanded and titered according to standard protocols (Earl et al., 2001). For experiments using VACV-OVA, skin scarification was performed as previously described (Liu et al., 2010). Briefly, three days after intradermal implantation of 1×10^6 B16-OVA cells (Day 3), 2×10^6 viral p.f.u. were applied to the tail in 5uL which was then scarified with 15 scratches from right to left and an additional 15 scratches from left to right.

Tissue Digestion of skin draining LNs and Spleens

In experiments isolating DCs from either skin draining LNs or spleens, tissues were ballooned and/or teased apart, and incubated for 25 min at 37°C in Collagenase D (400 U/ml, Roche) in Hanks' Balanced Salt Buffer containing Ca^{2+} (Invitrogen). After incubation, EDTA was added to a final concentration of 10 mM EDTA for 5 min at 37°C for disruption of DC–T cell complexes. For microarray sample preparation migDCs were flow sorted from n = 3 individual IFNγR1$^{-/-}$, IL27Rα$^{-/-}$, and C57BL/6J control mice after collagenase D digestion of pooled skin draining LNs on IAIE^{hi} CD11c^{int} selection following size and live/dead exclusion. RNA was prepared by standard methods using Trizol (Invitrogen), and further purified using RNeasy MinElute clean up (QIAGEN). Purity analysis was done using the Eukaryote Total RNA Pico Series II (Agilent). RNA was amplified and hybridized on the Affymetrix Mouse ST chips version 2.0.

Flow Cytometry Staining and Antibodies

All flow cytometric staining was performed on ice as described (Anandasabapathy et al., 2011). Cells were stained with Aqua Live/ Dead dye in PBS (Molecular Probes, Life Technologies), followed by extracellular staining in PBS containing 2% FCS (FACS Buffer) on ice, with subsequent fixation/permeabilization prior to staining for intracellular proteins. For intracellular cytokine analysis, cells were stimulated with cognate peptide for 1 hr prior to the addition of 10 μM Brefeldin A for five additional hours. The following murine and human antibodies were obtained from BD, eBioscience, or BioLegend: Anti: murine CD3 (eBio500A2), CD4 (RM4-5), CD8 (53-6.7), IFNγ (XMG1.2), TNFα (MP6-XT22), IL-2 (JES6-5H4), CD45 (30-F11), CD11b (M1/70), B220 (RA3-6B2), CD19 (eBio1D3), NK1.1 (PK136), FoxP3 (FJK-16S), IAIE (M5/114.15.2); anti human: BDCA1 (L161), BDCA3 (AD5), CD20 (2H7), CD66b (G10F5), CD56 (HCD56), CD11c (Bly6), CD14 (RM052), CD45 (HI30), HLA (L243). In murine experiments examining FoxP3 expression, fixation was performed using fixative and the manufacturers protocol from eBioscience, all other experiments utilized Fix/Perm from BD Biosciences.

Western Blot analysis

Western blot analysis of skin draining LN migDC and cDC. Mice were treated every other day by intraperitonial injection of 10ng recombinant human Flt3L for twelve days prior to LN digestion and FACS sorting. For western blot analysis of protein levels in DCs following in vitro culture, Flt3L derived BMDCs were generated by culture of total bone marrow cells supplemented with 100ng/ml Flt3L for 7 days. Cultures were harvested at 0 hr or treated with 200ng/mL of IFNγ for 24 hr or 48 hr. Western blotting was conducted with the follow

antibodies: SOCS2, Abcam; β–actin (AC-15), Sigma. Cells were lysed in modified RIPA buffer containing 50 mM Tris (pH 7.4), 1% NP-40,150 mM NaCl, 1 mM EDTA, 1 mM Na_3VO_4, and protease and phosphatase inhibitor cocktail (Life Technologies). Protein lysates were quantified using protein assay dye reagent (Bio-Rad). Equal amounts of proteins were separated by precast Tris-HCl SDS-polyacrylamide gel (Lonza), transferred to nitrocellulose membrane (Amersham), and incubated with primary antibodies in 1× TBS-T containing 5% non-fat dry milk overnight at 4°C. After washing the membranes in 1× TBS-T, membranes were incubated with horseradish peroxidase (HRP)-conjugated secondary antibodies for 1 hr at RT, binding of the primary antibodies were detected using an enhanced chemiluminescence substrate (Life Technologies).

Immunofluorescence

For immunofluorescence, frozen sections from biopsies of patients with common nevi, dysplastic nevi and primary malignant melanomas were fixed with acetone and blocked in 10% normal goat serum (Vector Laboratories) for 30 min. The tissue sections were incubated with mouse anti-human CD11c (clone Bly6, BD PharMingen) and rabbit anti-human SOCS2 (clone EPR2588(2), LifeSpan Biosciences), overnight at 4°C. The tissues were then amplified with goat anti-mouse Alexa Fluor 488 (Invitrogen, Eugene, OR, USA) and goat anti-rabbit Rhodamine Red X (Invitrogen, Eugene, OR, USA), for 30 min the next day. Images were acquired using the appropriate filters of a Zeiss Axioplan 2 widefield fluorescence microscope with a Plan Neofluar 20 9 0.7 numerical aperture lens and a Hamamatsu Orca ER cooled charge-coupled device camera, controlled by METAVUE software (MDS Analytical Technologies, Downington, PA, USA). Images in each figure are presented both as single color stains (green and red) located above the merged image, so that localization of two markers on similar or different cells can be appreciated. Cells that co-express the two markers in a similar location are yellow in color. A white line denotes the junction between epidermis and the dermis.

Genomics

Microarray analysis

Microarray analysis was carried out using the statistical language R and available Gene Expression Omnibus (GEO) datasets: 35459, 49358, 53588, 60782, 66970, 18686, and 32407. All work on pigmented lesion specimens (nevi and melanoma) was IRB approved at Rockefeller University and obtained by informed consent and includes previously published data sets GEO: GSE53223 for common and dysplastic nevi and new data set GEO: GSE100050 for normal skin and melanoma. Analysis was carried out using the statistical language R (www.R-project.org) and its available packages. Normalized expression data from the GEO datasets was accessed directly from R package GEOquery. Statistical analysis of each dataset was carried out anew using linear models in the limma framework and when samples in a given experiment were paired, a mixed model approach was used. In general once the model was fitted, the differences between groups was assessed using contrasts with A moderated t test. Resultant p values were adjusted for multiple comparisons across markers using the Benjamini-Hochberg approach, which controls the False Discovery Rate. Gene Annotation: each dataset was annotated using the respective R annotation packages.

Unsupervised hierarchical clustering was carried out using the euclidean with the average agglomeration algorithm. Expression of the clustered genes is represented as heatmaps with a scaling by gene. Correlation between the log2 FCHs across experiments was carried out using Pearson pairwise correlation, follow by unsupervised clustering based on euclidean distance.

Over-representation analysis

We identified gene-sets that overlap with the 227 list by using a hypergeometric test using hallmark, C2, and C7 collections from Molsigdb (https://www.broadinstitute.org/msigdb) and Krueger skin collection sets. p values representing the significance of the overlap were adjusted using the Benjamini-Hochberg approach to control for false discovery rate.

Z-scoring/Gene Set Variation analysis

The activity of entire signaling pathways for each sample was quantified by using a per-sample GSEA-like method. GSVA (Gene Set Variation Analysis) is an unsupervised sample-wise enrichment method (Hänzelmann et al., 2013). Enrichment scores were obtained using the z-score method previously described (Lee et al., 2008) and available in the GSVA *R* package. This method computes a linear combination of normalized expressions with weights in the combination being defined as $1/\sqrt{k}$ for k being the number of genes in the pathway. The per-sample enrichment scores are then compared across different groups for each of the relevant experiments. The null distribution of the Z-scores was obtained by conduction of a simulation study. For each gene set of a give size k, we randomly selected a set of k genes and its calculated z-score.

SEEK analysis

We entered the 227-gene signature as query into SEEK to compute the co-expression score of 227 genes and its significance for each dataset in the large SEEK compendia composed of thousands of datasets. Default settings were used. For our purpose, we excluded small datasets containing less than 10 samples which may give unreliable scores. Cutoff of p = 0.001 was used to define co-expressed datasets for the 227-gene query. To identify the MeSH terms (such as neoplasms, ulcerative colitis) which may be overrepresented among top SEEK-prioritized datasets, we computed the hypergeometric overlap p value:

$$P(X \geq k) = \sum_{i=k \ldots K} \frac{\binom{K}{i}\binom{N-K}{n-i}}{\binom{N}{n}}$$

where N is the total datasets with any MeSH annotations, K is the datasets annotated to a given MeSH term, n is the depth in the dataset list, and k is the datasets within the list at depth n annotated to a given MeSH term.

Pan Cancer TCGA analysis

TCGA RNaseq level 3 processed data and the corresponding clinical annotations were obtained from the UCSC cancer genome browser (https://genome-cancer.ucsc.edu/proj/site/hgHeatmap/). Gene level expression estimates are reported using RSEM normalized counts and were restricted to only include those sequenced on the Illumina HiSeq platform from the same center, UNC. For each sample the average expression of a signature was calculated by taking the geometric mean of the expression values for all genes in the signature. Using these per sample scores the Pearson correlation between 227 and IFNγ was calculated for each tumor type. For SKCM, patients were stratified into high, medium, and low groups using quantiles, with the high group corresponding to the upper quartile, the low group the lower quartile, and medium the remaining two quartiles. All statistical tests for these data were run using R version 3.1.1.

Whole transcriptome amplification, library preparation, and scRNA-Seq

Whole transcriptome amplification (WTA) from single-cell lysates was performed using Smart-Seq2 as previously described (Trombetta et al., 2014) (Tirosh et al., 2016) except Maxima Reverse Transcriptase was used in place of SuperScript II (both from Life Technologies). Libraries were sequenced on an Illumina NextSeq 500 (30 base pair paired-end reads) to an average depth of 1.1M ± 0.06M reads.

Processing of RNA-Seq data

Following sequencing, BAM files were converted to merged, demultiplexed FASTQ files, and mapped to the UCSC hg19 human transcriptome, as previously described (Tirosh et al., 2016) We included cells in our analysis: 1. with greater than 2,000 genes detected; 2. whose average expression of a curated list of housekeeping genes was greater than $\log_2(\text{TPM}) = 4$; and, 3. which had greater than 20% alignment to the h19 transcriptome. We chose genes, meanwhile, that were expressed in at least 15% of all selected cells for downstream analysis.

Importantly, here, TPM values were not divided by 10. When evaluating the average expression of populations of single cells from Tirosh et al., the expression level for each gene in each cell was multiplied by 10 to enable direct comparison.

t-SNE analysis

A matrix of genes (rows) by cells (columns) was loaded into the Seurat R package version 1.2 in R version 3.1.1 (Satija et al., 2015) and for all genes, the arithmetic mean and pairwise dispersion (mean-normalized standard deviation) were calculated. Genes with a mean log2(TPM) greater than 4 and z-scored dispersion higher than 1 were marked as “variable.” A principal components analysis was then run on all cells over variable genes. We selected principal components for downstream analysis by inspecting the fraction of total variance explained by each component and its significance as calculated using the Jackstraw algorithm implemented through Seurat (Chung and Storey, 2015). Principal components 1 through 4 were chosen as inputs for t-SNE based on cutoffs of greater than 1.5% variance explained and p values less than 10^{-10} (FDR <0.01). Component 6 was also included, as inspection of the top genes correlated with this component revealed separation of PDCs and

mDCs (Table S7A) t-SNE was performed over 2,400 iterations with a perplexity of 15 and visualized in R with Seurat.

Heatmaps for 227 signature

Differential expression across the genes in the 227 signature was calculated using the "find.markers" function in Seurat, running a likelihood ratio test over a parameterized bimodal distribution(McDavid et al., 2013). Heatmaps were then generated as previously described (Tirosh et al., 2016). Briefly, expression fold changes were calculated for each population and used to generate a heatmap of relative expression across each of two gene sets ("227 Up," and "227 Down." The rows (populations) were ordered by hierarchical clustering. Genes, meanwhile, were first assigned to the population to which they had the highest fold difference. Then a modified silhouette score was tasked to rank the genes within each population. Silhouette scoring ($S_{x,i}$) was performed by calculating, for each gene i:

$$S_{x,i}=\sum_{j} x_i - x_j$$

where x is the population assigned to gene i and j includes all other genes in population x. Next, $S_{y,i}$, the sum of the differences in expression between x_i and y_j, was determined:

$$S_{y,i}=\sum_{j} x_i - y_j$$

where j are all genes belonging to all other populations y. The magnitude of $S_{x,i}/S_{y,i}$ was calculated for all genes, and used to rank the genes in terms of similarity within a population. When ordered by population, the resulting heatmap displays genes most closely associated with each population ranked in succession.

Intra-population correlation analysis

Composite scores for the upregulated and downregulated genes for the 227 and IFNγ gene sets were constructed by averaging the weighted gene expression for each single cell as previously described (Shalek et al., 2014). The Spearman correlation between the 227-gene signature for a cell and the IFNγ gene signature in the same cell was calculated for both the upregulated and downregulated scores. Then, the cells were permuted in each population so the correlation was calculated between the 227-gene score and IFNγ score of different cells. This was repeated 100 times, and the average correlation was plotted.

Inter-population correlation analysis

To account for differences in the number of cells across various populations, 100 random permutations of 40 cells were selected from each and averaged to create 100 40-cell in silico "bulk" scores for both the 227-gene and IFNγ signatures. The Spearman correlation between the 227-gene and IFNγ score of each in silico "bulk" with itself and with other in

silico “bulks” was calculated. A heatmap was generated in R using heatmap.2 to visualize these correlations.

Quantification and Statistical Analysis

Statistical analysis

Analysis of ex vivo T cell responses for vaccine, contact sensitization and tumor analyses was conducted using Prism software and depicts mean ± standard error of the mean (SEM). Data are presented as mean ± standard error of the mean, or mean ± standard deviation. Group sizes were determined based on the results of preliminary experiments without pre-determination of sample size. Preliminary experiments were performed to determine requirements for sample size, taking into account resources available and ethical, reductionist animal use. Mice were randomly assigned to groups. Mouse studies were not performed in a blinded fashion. Generally, each mouse of the different experimental groups is reported. Statistical analysis using the two-tailed unpaired Student's t test, under the untested assumption of normality, was calculated using Prism software (GraphPad), with significance reported for $p < .05$.

227 t tests and Venn diagram

Processed expression data and the corresponding clinical annotations were obtained from the Gene Expression Omnibus Repository (GEO, https://www.ncbi.nlm.nih.gov/geo/). All data were normalized and logged transformed (base 2). The 227-gene signature was extracted from each of the dataset for further analysis. Genes that were differentially expressed across the control and experimental groups were identified using t tests with cutoff of $p < 0.05$ (MeV_4_8 Version 10.2). Expression data from GEO: GSE35459, GEO: GSE49358, GEO: GSE53588, GEO: GSE60782, and GEO: GSE66970 were analyzed using an unpaired t test. GEO: GSE18686 and GEO: GSE32704 data were analyzed using a paired t test. Please see Table S4 for comparison sets.

Data and Software Availability

The accession number for murine IFNGR1-/- migratory DCs, IL-27Ra-/- migratory DCs, and wildtype migratory DCs newly reported in this paper is GEO: GSE98994. Data sets dysplastic nevi and common melanocytic nevi previously reported are located in GEO: GSE53223. New data sets for primary human melanoma and normal skin are reported in GEO: GSE100050. Raw and processed single-cell RNA-seq data is available at GEO: GSE72056. The dbGAP accession number for the single-cell sequencing data from $BDCA3^+$, $BDCA1^+$, and monocyte populations newly reported in this paper is still pending and will be updated in the online version of the paper once it is available. Until then, requests can be made directly to the authors. Processed single-cell and bulk RNA-seq data is available at GEO: GSE######.

Supplementary Material

Refer to Web version on PubMed Central for supplementary material.

Acknowledgments

Doug Hilton and Warren Alexander generously provided *SOCS2*$^{-/-}$ mice. The laboratories of Arlene Sharpe and Charles Drake provided B16-OVA and EL4-OVA tumor lines. We are grateful to Celldex for recombinant Flt3L, Steve Reed and Infectious Disease Research Institute for GLA, and Dev Manoli for critical reading of the manuscript. C.N. was supported by a 5T32AR007098 Dermatology Training Grant. B.I. was supported by the DFCI Wong Family Award for Translational Cancer Research. N.G. was supported by a T32GM07739 MSTP Grant. A.K.S. was supported by the Searle Scholars Program, the Beck-man Young Investigator Program, and the NIH New Innovator Award DP2OD020839. N.A., Y.L., and C.N. were supported by the Melanoma Research Alliance-BWH Department of Dermatology combined grant, the Cancer Research Institute, the Klarman Family Foundation, and the National Institute of Arthritis and Musculoskeletal and Skin Disease R01AR070234 and K23 AR063461 (to N.A). A.R. is on the scientific advisory board for ThermoFisher Scientific, Syros Pharmaceuticals, and Driver Group. J.G.K. is a consultant for Biogen. L.G. was a consultant for Foundation Medicine, No-vartis, Boehringer Ingelheim, Eli Lilly, an equity holder in Foundation Medicine, and a member of the scientific advisory board at Warp Drive. L.G. also received grant support from Novartis. L.G. is now an employee of Eli Lilly and Company.

References

Anandasabapathy N, Victora GD, Meredith M, Feder R, Dong B, Kluger C, Yao K, Dustin ML, Nussenzweig MC, Steinman RM, Liu K. Flt3L controls the development of radiosensitive dendritic cells in the meninges and choroid plexus of the steady-state mouse brain. J Exp Med. 2011; 208:1695–1705. [PubMed: 21788405]

Anandasabapathy N, Feder R, Mollah S, Tse SW, Longhi MP, Mehandru S, Matos I, Cheong C, Ruane D, Brane L, et al. Classical Flt3L-dependent dendritic cells control immunity to protein vaccine. J Exp Med. 2014; 211:1875–1891. [PubMed: 25135299]

Askenase MH, Han SJ, Byrd AL, Morais da Fonseca D, Bouladoux N, Wilhelm C, Konkel JE, Hand TW, Lacerda-Queiroz N, Su XZ, et al. Bone-Marrow-Resident NK Cells Prime Monocytes for Regulatory Function during Infection. Immunity. 2015; 42:1130–1142. [PubMed: 26070484]

Baratin M, Foray C, Demaria O, Habbeddine M, Pollet E, Maurizio J, Verthuy C, Davanture S, Azukizawa H, Flores-Langarica A, et al. Homeostatic NF-κB Signaling in Steady-State Migratory Dendritic Cells Regulates Immune Homeostasis and Tolerance. Immunity. 2015; 42:627–639. [PubMed: 25862089]

Bonifaz LC, Bonnyay DP, Charalambous A, Darguste DI, Fujii S, Soares H, Brimnes MK, Moltedo B, Moran TM, Steinman RM. In vivo targeting of antigens to maturing dendritic cells via the DEC-205 receptor improves T cell vaccination. J Exp Med. 2004; 199:815–824. [PubMed: 15024047]

Chen M, Wang YH, Wang Y, Huang L, Sandoval H, Liu YJ, Wang J. Dendritic cell apoptosis in the maintenance of immune tolerance. Science. 2006; 311:1160–1164. [PubMed: 16497935]

Chung NC, Storey JD. Statistical significance of variables driving systematic variation in high-dimensional data. Bioinformatics. 2015; 31:545–554. [PubMed: 25336500]

Dalod M, Chelbi R, Malissen B, Lawrence T. Dendritic cell maturation: functional specialization through signaling specificity and transcriptional programming. EMBO J. 2014; 33:1104–1116. [PubMed: 24737868]

Dunn GP, Koebel CM, Schreiber RD. Interferons, immunity and cancer immunoediting. Nat Rev Immunol. 2006; 6:836–848. [PubMed: 17063185]

Earl PL, Cooper N, Wyatt LS, Moss B, Carroll MW. Preparation of cell cultures and vaccinia virus stocks. Curr Protoc Protein Sci. 2001; Chapter 5

Elder DE. Melanoma progression. Pathology. 2016; 48:147–154. [PubMed: 27020387]

Frucht DM, Fukao T, Bogdan C, Schindler H, O'Shea JJ, Koyasu S. IFN-gamma production by antigen-presenting cells: mechanisms emerge. Trends Immunol. 2001; 22:556–560. [PubMed: 11574279]

Fuentes-Duculan J, Suárez-Fariñas M, Zaba LC, Nograles KE, Pierson KC, Mitsui H, Pensabene CA, Kzhyshkowska J, Krueger JG, Lowes MA. A subpopulation of CD163-positive macrophages is classically activated in psoriasis. J Invest Dermatol. 2010; 130:2412–2422. [PubMed: 20555352]

Greenhalgh CJ, Rico-Bautista E, Lorentzon M, Thaus AL, Morgan PO, Willson TA, Zervoudakis P, Metcalf D, Street I, Nicola NA, et al. SOCS2 negatively regulates growth hormone action in vitro and in vivo. J Clin Invest. 2005; 115:397–406. [PubMed: 15690087]

Haniffa M, Shin A, Bigley V, McGovern N, Teo P, See P, Wasan PS, Wang XN, Malinarich F, Malleret B, et al. Human tissues contain CD141hi cross-presenting dendritic cells with functional homology to mouse CD103+ nonlymphoid dendritic cells. Immunity. 2012; 37:60–73. [PubMed: 22795876]

Hänzelmann S, Castelo R, Guinney J. GSVA: gene set variation analysis for microarray and RNA-seq data. BMC Bioinformatics. 2013; 14:7. [PubMed: 23323831]

Harden JL, Gu T, Kilinc MO, Rowswell-Turner RB, Virtuoso LP, Egilmez NK. Dichotomous effects of IFN-γ on dendritic cell function determine the extent of IL-12-driven antitumor T cell immunity. J Immunol. 2011; 187:126–132. [PubMed: 21632715]

Hoeffel G, Chen J, Lavin Y, Low D, Almeida FF, See P, Beaudin AE, Lum J, Low I, Forsberg EC, et al. C-Myb(+) erythro-myeloid progenitor-derived fetal monocytes give rise to adult tissue-resident macrophages. Immunity. 2015; 42:665–678. [PubMed: 25902481]

Iborra S, Martínez-López M, Khouili SC, Enamorado M, Cueto FJ, Conde-Garrosa R, Del Fresno C, Sancho D. Optimal Generation of Tissue-Resident but Not Circulating Memory T Cells during Viral Infection Requires Crosspriming by DNGR-1(+) Dendritic Cells. Immunity. 2016; 45:847–860. [PubMed: 27692611]

Inaba K, Turley S, Yamaide F, Iyoda T, Mahnke K, Inaba M, Pack M, Subklewe M, Sauter B, Sheff D, et al. Efficient presentation of phagocytosed cellular fragments on the major histocompatibility complex class II products of dendritic cells. J Exp Med. 1998; 188:2163–2173. [PubMed: 9841929]

Kaplan DH, Shankaran V, Dighe AS, Stockert E, Aguet M, Old LJ, Schreiber RD. Demonstration of an interferon gamma-dependent tumor surveillance system in immunocompetent mice. Proc Natl Acad Sci USA. 1998; 95:7556–7561. [PubMed: 9636188]

Kushwah R, Hu J. Dendritic cell apoptosis: regulation of tolerance versus immunity. J Immunol. 2010; 185:795–802. [PubMed: 20601611]

Lee E, Chuang HY, Kim JW, Ideker T, Lee D. Inferring pathway activity toward precise disease classification. PLoS Comput Biol. 2008; 4:e1000217. [PubMed: 18989396]

Liu L, Zhong Q, Tian T, Dubin K, Athale SK, Kupper TS. Epidermal injury and infection during poxvirus immunization is crucial for the generation of highly protective T cell-mediated immunity. Nat Med. 2010; 16:224–227. [PubMed: 20081864]

Ma DY, Clark EA. The role of CD40 and CD154/CD40L in dendritic cells. Semin Immunol. 2009; 21:265–272. [PubMed: 19524453]

Martin SF. Induction of contact hypersensitivity in the mouse model. Methods Mol Biol. 2013; 961:325–335. [PubMed: 23325654]

Mascanfroni ID, Yeste A, Vieira SM, Burns EJ, Patel B, Sloma I, Wu Y, Mayo L, Ben-Hamo R, Efroni S, et al. IL-27 acts on DCs to suppress the T cell response and autoimmunity by inducing expression of the immunoregulatory molecule CD39. Nat Immunol. 2013; 14:1054–1063. [PubMed: 23995234]

McDavid A, Finak G, Chattopadyay PK, Dominguez M, Lamoreaux L, Ma SS, Roederer M, Gottardo R. Data exploration, quality control and testing in single-cell qPCR-based gene expression experiments. Bio-informatics. 2013; 29:461–467.

McGovern N, Schlitzer A, Gunawan M, Jardine L, Shin A, Poyner E, Green K, Dickinson R, Wang XN, Low D, et al. Human dermal $CD14^{+}$ cells are atransient populationof monocyte-derived macrophages. Immunity. 2014; 41:465–477. [PubMed: 25200712]

Mellor AL, Munn DH. Creating immune privilege: active local suppression that benefits friends, but protects foes. Nat Rev Immunol. 2008; 8:74–80. [PubMed: 18064049]

Miller JC, Brown BD, Shay T, Gautier EL, Jojic V, Cohain A, Pandey G, Leboeuf M, Elpek KG, Helft J, et al. Deciphering the transcriptional network of the dendritic cell lineage. Nat Immunol. 2012; 13:888–899. [PubMed: 22797772]

Ohl L, Mohaupt M, Czeloth N, Hintzen G, Kiafard Z, Zwirner J, Blankenstein T, Henning G, Förster R. CCR7 governs skin dendritic cell migration under inflammatory and steady-state conditions. Immunity. 2004; 21:279–288. [PubMed: 15308107]

Patel AP, Tirosh I, Trombetta JJ, Shalek AK, Gillespie SM, Wakimoto H, Cahill DP, Nahed BV, Curry WT, Martuza RL, et al. Single-cell RNA-seq highlights intratumoral heterogeneity in primary glioblastoma. Science. 2014; 344:1396–1401. [PubMed: 24925914]

Rico-Bautista E, Flores-Morales A, Fernández-Pérez L. Suppressor of cytokine signaling (SOCS) 2, a protein with multiple functions. Cytokine Growth Factor Rev. 2006; 17:431–439. [PubMed: 17070092]

Rothhammer V, Mascanfroni ID, Bunse L, Takenaka MC, Kenison JE, Mayo L, Chao CC, Patel B, Yan R, Blain M, et al. Type I interferons and microbial metabolites of tryptophan modulate astrocyte activity and central nervous system inflammation via the aryl hydrocarbon receptor. Nat Med. 2016; 22:586–597. [PubMed: 27158906]

Satija R, Farrell JA, Gennert D, Schier AF, Regev A. Spatial reconstruction of single-cell gene expression data. Nat Biotechnol. 2015; 33:495–502. [PubMed: 25867923]

Schlitzer A, Sivakamasundari V, Chen J, Sumatoh HR, Schreuder J, Lum J, Malleret B, Zhang S, Larbi A, Zolezzi F, et al. Identification of cDC1- and cDC2-committed DC progenitors reveals early lineage priming at the common DC progenitor stage in the bone marrow. Nat Immunol. 2015; 16:718–728. [PubMed: 26054720]

Schroder K, Hertzog PJ, Ravasi T, Hume DA. Interferon-gamma: an overview of signals, mechanisms and functions. J Leukoc Biol. 2004; 75:163–189. [PubMed: 14525967]

Shalek AK, Satija R, Shuga J, Trombetta JJ, Gennert D, Lu D, Chen P, Gertner RS, Gaublomme JT, Yosef N, et al. Single-cell RNA-seq reveals dynamic paracrine control of cellular variation. Nature. 2014; 510:363–369. [PubMed: 24919153]

Snyder A, Makarov V, Merghoub T, Yuan J, Zaretsky JM, Desrichard A, Walsh LA, Postow MA, Wong P, Ho TS, et al. Genetic basis for clinical response to CTLA-4 blockade in melanoma. N Engl J Med. 2014; 371:2189–2199. [PubMed: 25409260]

Steinman RM. Decisions about dendritic cells: past, present, and future. Annu Rev Immunol. 2012; 30:1–22. [PubMed: 22136168]

Stern RS. Prevalence of a history of skin cancer in 2007: results of an incidence-based model. Arch Dermatol. 2010; 146:279–282. [PubMed: 20231498]

Tamoutounour S, Guilliams M, Montanana Sanchis F, Liu H, Terhorst D, Malosse C, Pollet E, Ardouin L, Luche H, Sanchez C, et al. Origins and functional specialization of macrophages and of conventional and monocyte-derived dendritic cells in mouse skin. Immunity. 2013; 39:925–938. [PubMed: 24184057]

Taube JM, Young GD, McMiller TL, Chen S, Salas JT, Pritchard TS, Xu H, Meeker AK, Fan J, Cheadle C, et al. Differential Expression of Immune-Regulatory Genes Associated with PD-L1 Display in Melanoma: Implications for PD-1 Pathway Blockade. Clin Cancer Res. 2015

Tirosh I, Izar B, Prakadan SM, Wadsworth MH 2nd, Treacy D, Trom-betta JJ, Rotem A, Rodman C, Lian C, Murphy G, et al. Dissecting the multicellular ecosystem of metastatic melanoma by single-cell RNA-seq. Science. 2016; 352:189–196. [PubMed: 27124452]

Tomasetti C, Vogelstein B. Cancer etiology. Variation in cancer risk among tissues can be explained by the number of stem cell divisions. Science. 2015; 347:78–81. [PubMed: 25554788]

Trombetta JJ, Gennert D, Lu D, Satija R, Shalek AK, Regev A. Preparation of Single-Cell RNA-Seq Libraries for Next Generation Sequencing. Current protocols in molecular biology. 2014; 107:4.22 21–17. [PubMed: 24984854]

Waithman J, Allan RS, Kosaka H, Azukizawa H, Shortman K, Lutz MB, Heath WR, Carbone FR, Belz GT. Skin-derived dendritic cells can mediate deletional tolerance of class I-restricted self-reactive T cells. J Immunol. 2007; 179:4535–4541. [PubMed: 17878350]

Wilson NS, Young LJ, Kupresanin F, Naik SH, Vremec D, Heath WR, Akira S, Shortman K, Boyle J, Maraskovsky E, et al. Normal proportion and expression of maturation markers in migratory dendritic cells in the absence of germs or Toll-like receptor signaling. Immunol Cell Biol. 2008; 86:200–205. [PubMed: 18026177]

Yeste A, Takenaka MC, Mascanfroni ID, Nadeau M, Kenison JE, Patel B, Tukpah AM, Babon JA, DeNicola M, Kent SC, et al. Tolerogenic nanoparticles inhibit T cell-mediated autoimmunity through SOCS2. Sci Signal. 2016; 9:ra61. [PubMed: 27330188]

Zaidi MR, Merlino G. The two faces of interferon-γ in cancer. Clin Cancer Res. 2011; 17:6118–6124. [PubMed: 21705455]

Zhu Q, Wong AK, Krishnan A, Aure MR, Tadych A, Zhang R, Corney DC, Greene CS, Bongo LA, Kristensen VN, et al. Targeted exploration and analysis of large cross-platform human transcriptomic compendia. Nat Methods. 2015; 12:211–214. 3–214. [PubMed: 25581801]

Highlights

- Immune phagocytes share a conserved program during differentiation and tissue entry
- IFNγ is a critical instructive cue in the steady state
- IFNγ and tissue programming are co-opted across cancers and include SOCS2
- SOCS2 is a critical determinant of tumor-immune surveillance in dendritic cells

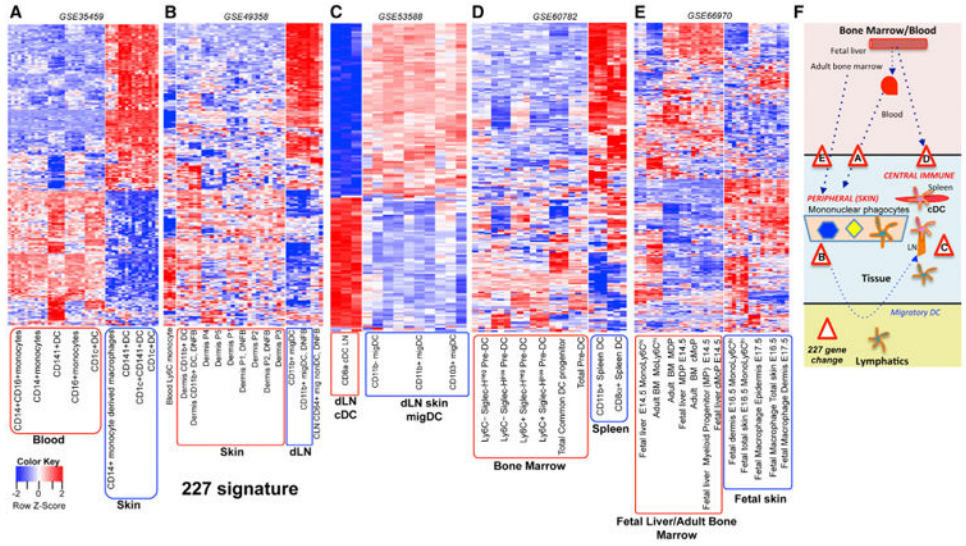

Figure 1. Enriched Expression of a Species-Conserved 227 Homeostatic Signature at Tissue Entry across Mononuclear Phagocyte Lineages and at Multiple Stages of Differentiation and Development

(A–E) 227-gene signatures were derived from classical DCs in datasets GEO: GSE35459 and GEO: GSE53588. Gene expression analysis was mapped across individual samples of mononuclear phagocytes in the following datasets: (A) GEO: GSE35459, comparing human blood DCs and monocytes to skin DCs and monocyte-derived macrophages; (B) GEO: GSE49358, comparing murine dermal DCs and monocytes to those that have migrated to the LN, with and without DNFB—a contact sensitizing agent; (C) GEO: GSE53588, comparing murine skin derived migDCs in LN to LN-resident cDCs from Flt3L treated mice; (D) GEO: GSE60782, comparing murine cDC progenitors (pre-DC subtypes) in bone marrow to differentiated spleen-resident cDCs; and (E) GEO: GSE66970, comparing embryonic liver and adult bone marrow mononuclear phagocyte progenitors to differentiated embryonic skin monocytes and macrophages.

(F) Schematic mapping of each analyzed set to the selected developmental transition or tissue-based comparison. Triangles indicate a defined transition in either progenitor differentiation or tissue entry as detailed in Table S1A.

See also Figure S1.

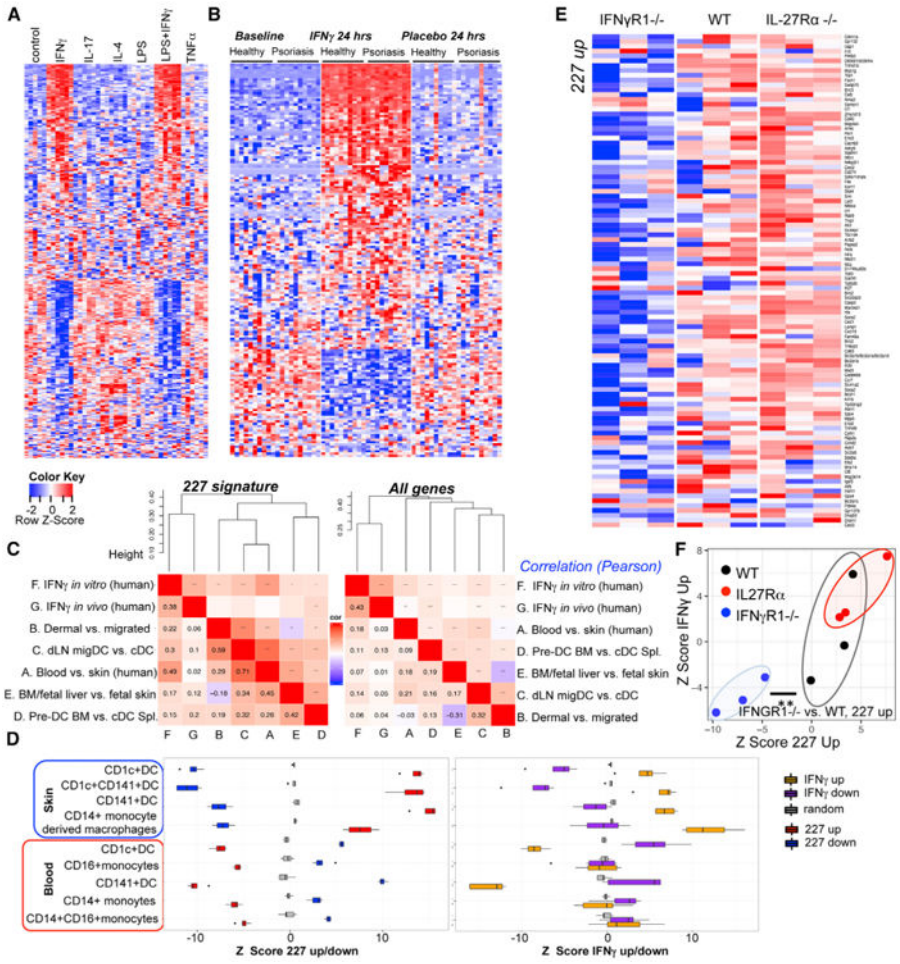

Figure 2. IFNγ Is Sufficient and Necessary to Induce 227-Gene Transcripts in Human Mononuclear Phagocytes and Human Skin

(A) 227-signature expression analysis of transcripts derived from paired PBMC specimens from six individuals. Human PBMCs were selected for monocytes by adherence, cultured for 7 days with M-CSF, and treated for 24 hr with (A) IFNγ, IL-17, IL-4, LPS, LPS + IFNγ, or TNFα (paired conditions per patient, GEO: GSE18686).

(B) 227-signature expression analysis in paired skin biopsy specimens obtained from 3 different sites of the same individual: normal healthy skin and skin taken 24 hr after either injection of IFNγ or injection of placebo (vehicle control) from 10 healthy individuals or psoriasis patients (GEO: GSE32407).

(C) Unsupervised hierarchical clustering based on the Pearson correlation of $\log_2$(FCH) for each defined comparison within each of the 7 datasets, testing genes within the 227 signatures (left) or all possible overlapping transcripts (right). Values in each cell represent the Pearson correlation and significance levels are represented as *p < 0.05, **p < 0.01, ***p < 0.001. Comparison sets are listed as follows: A. Blood versus skin (human), GEO: GSE35459. B. Dermal versus migrated, GEO: GSE49358. C. Draining LN skin migratory DC (migDC) versus LN resident CD8α cDC, GEO: GSE53588. D. Pre-DC from bone marrow versus cDC from spleen, GEO: GSE60782. E. Adult bone marrow and fetal liver embryonic progenitors versus macrophages and monocytes in fetal skin, GEO: GSE66970 F.

IFNγ and IFNγ + LPS versus all other treatments from human monocyte-derived macrophages in vitro, GEO: GSE18686. G. IFNγ injected skin versus placebo/ control from healthy human volunteers and psoriasis patients ex vivo, GEO: GSE32407.
(D) Distribution of the *Z* scores for GEO: GSE35459 samples comparing human blood DC and monocyte subsets to human skin DC or monocyte-derived macrophage subsets for 227 signature up (red) or down (blue) genes or an equivalent number of random probes (gray). Parallel comparison of human blood versus skin (left) of 1,217 IFNγ upregulated (orange) and 1210 IFNγ downregulated (purple) signature correlations (right) or an equivalent number of random probes (gray) (GEO: GSE18686, IFNγ and IFNγ + LPS specimens versus all other conditions).
(E) Gene expression of the 227 upregulated signature module in migDC isolated from IFNγR1$^{-/-}$, WT, and IL27Rα$^{-/-}$ mice. Each column represents migDC sorted from one mouse and processed as three distinct technical replicates.
(F) GSVA. Association between *Z* score of IFNγ and 227 upregulated signatures (r = 0.9, CI =0.63-0.98) in individual IFNγR1$^{-/-}$ (blue), WT (black), and IL27Rα$^{-/-}$ (red) mice. Oval grouping of samples of migDC by condition, depicting n = 3 individual mice. Significance in loss of the 227 upregulated signature as compare to WT mice is noted **p < .01.
See also Figure S2.

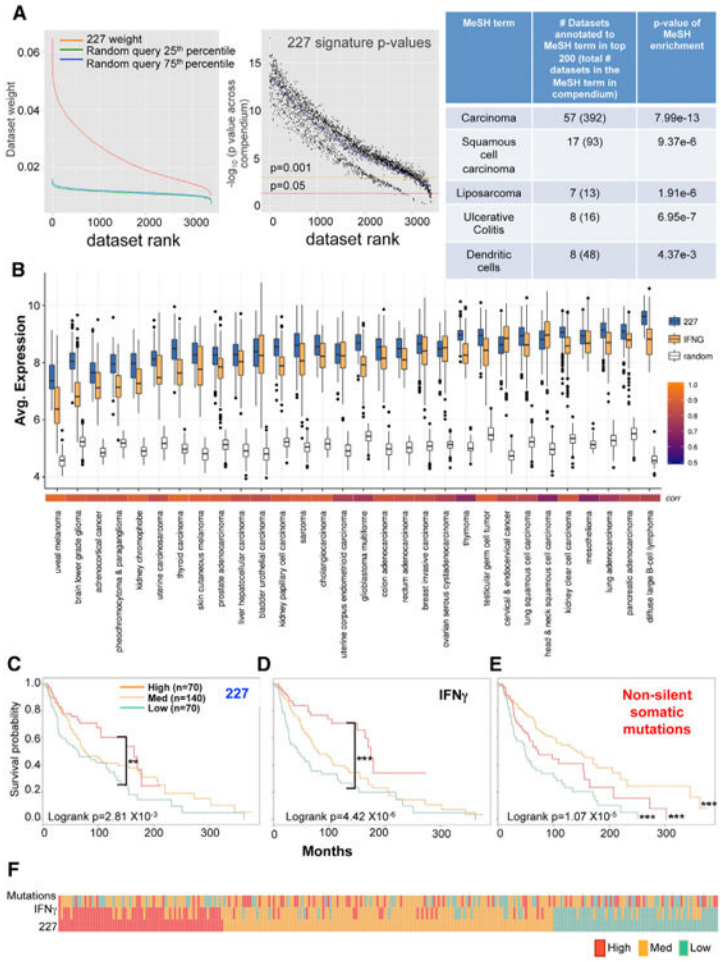

Figure 3. IFNγ-Directed Transcripts Co-enriched and Correlate with 227 Signature Genes across Multiple Human Cancers and Stratify Human Melanoma Survival

(A) SEEK analysis was performed comparing average 25th and 75th quartile random queries to 227-signature genes across the Gene Expression Omnibus and Cancer Genome Atlas datasets. Per dataset co-expression p values are plotted for 227 signatures demonstrating high levels of significance across thousands of datasets in the SEEK compendia. Among top 200 datasets prioritized, a significant portion of sets are associated with cancer, auto inflammatory disease (e.g., ulcerative colitis), and DCs.

(B) Top 150 transcripts taken from IFNγ signatures (irrespective of direction of change), 200 of 227 homeostatic signature genes, or 200 random probes were compared across primary human cancers (TCGA). Correlation scores between individual tumor specimens expressing the IFNγ signature and homeostatic 227 signature are color coded and depicted below the plots (0.5–1) per cancer subtype. Kaplan-Meier Survival analysis of TCGA level 4 skin cutaneous melanoma (SKCM) from 280 metastatic melanoma patients.

(C–E) High, medium, and low expression of either the (C) 227 signature, (D) IFNγ-dependent top 150 transcripts, or (E) non-silent somatic mutations were used to stratify patient survival.

(F) Comparison of patient samples classified by high, medium, or low average expression for the IFNγ signature, 227 signature, or non-silent somatic mutations.

See also Figure S3.

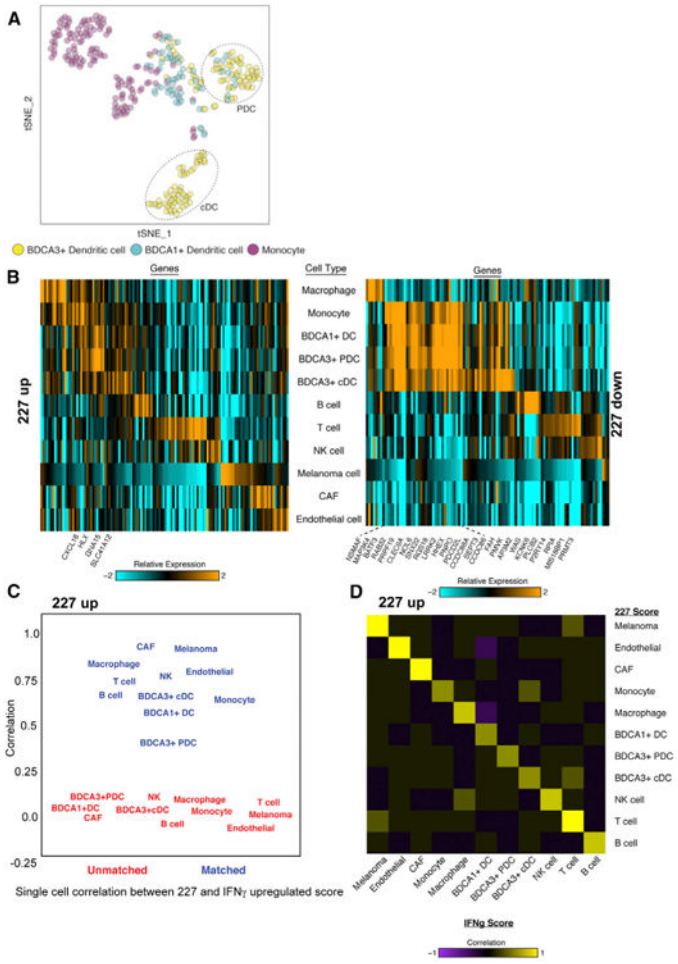

Figure 4. Single-Cell RNA-Seq Reveals 227 Programming in Mononuclear Phagocytes and Close Per-Cell and Population-Based Correlation between 227 Homeostatic Programming and IFNγ

(A) Transcriptomes of 333 BDCA1$^+$ DC, BDCA3$^+$DC, and monocytes from a patient with melanoma visualized by tSNE. Differential gene expression between two annotated BDCA3$^+$ dendritic cell clusters (Table S7A) shows that they are PDC-like and cDCs.

(B) Heatmaps representing relative single-cell expression of the up (left) and downregulated (right) genes that comprise the 227 signature annotated by single-cell populations previously assayed (Tirosh et al., 2016), along with additional populations of monocytes and DC examined here. Genes with expression fold change greater than 1.5 in at least two of four populations are annotated below the heatmaps: monocyte, BDCA1$^+$ DC, BDCA3$^+$ PDC, and BDCA3$^+$ cDC.

(C) Correlation of the upregulated gene score in the 227-signature of a single cell and the IFNγ gene signature of the same cell (matched) or the average of the other single cells from within the same population (unmatched). The matched correlation is higher than the unmatched correlation for every population (p value < 0.001, paired t test).

(D) Correlation of the upregulated gene score in the 227-gene signature and IFNγ gene signatures between in silico “bulk” averages of each population. The upregulated gene score of the 227-gene signature and IFNγ signature of each population is most correlated with its own IFNγ signature and 227-gene signature, respectively (p value < 0.003; Welch's t test).

See also Figure S4.

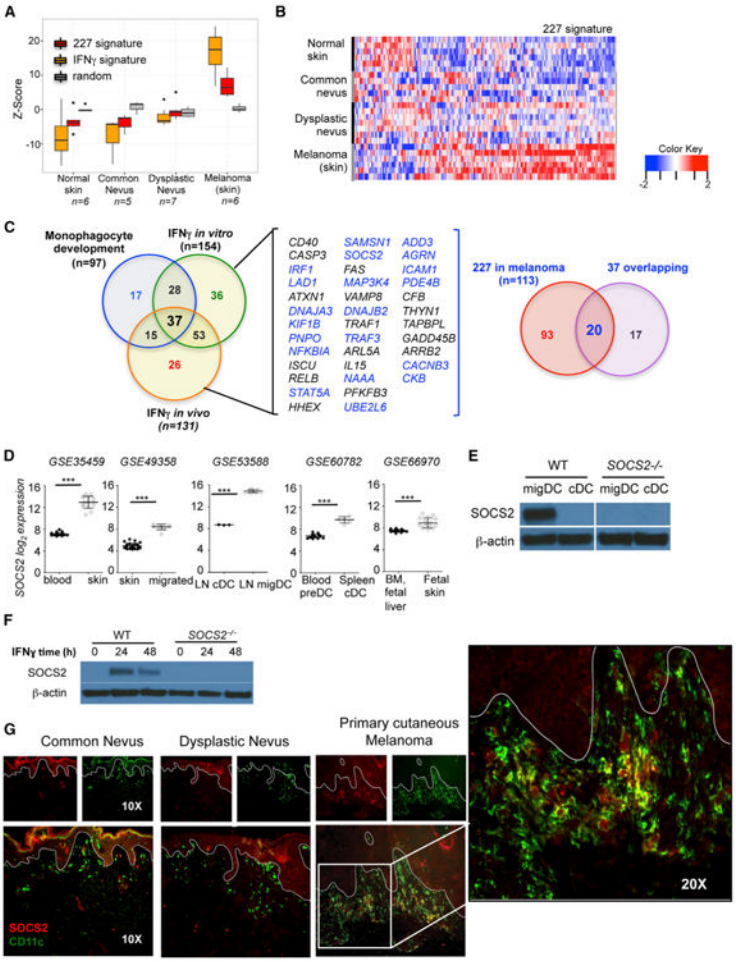

Figure 5. 227-Gene Signatures, IFNγ-Specific Signatures, and SOCS2 Are Closely Associated with Early Human Primary Cutaneous Melanoma

(A) *Z* score comparing overall expression levels for IFNγ- and 227-gene signatures in skin biopsies taken from normal skin (n = 6 patients), common nevi (n = 5 patients), dysplastic nevi (n = 7 patients), or primary cutaneous melanoma (n = 6 patients).

(B) Corresponding 227-signature heatmap analysis.

(C) Venn diagram overlapping 227 signature genes with a statistically significant intersection (n = 37) across all 5 mononuclear phagocyte transitions (n= 97), with IFNγ in vitro (n = 154) and in vivo (n = 131) treatments (left). Venn diagram of 227 genes in melanoma (n = 113) overlapping the 37 genes intersecting all developmental transitions and those induced by IFNγ in vitro and in vivo (right). The list of 37 genes includes those overlapping the 113 of 227 signatures induced in melanoma (blue).

(D) Log_2 expression of *SOCS2* transcripts in human (GEO: GSE35459) and murine (GEO: GSE49358, GEO: GSE53588, GEO: GSE60782, GEO: GSE66970) DC ormonocyte/ macrophage subsets defined by groups.

(E) Expression of SOCS2 protein in migDCs and cDCs isolated from skin draining LNs from Flt3L treated mice (n = one of two representative experiments).

(F) SOCS2 and β–actin expression in cellular lysates of Flt3L-cultured murine BMDCs derived from WT or *SOCS2*$^{-/-}$ mice prepared prior to or 24 or 48 hr after IFNγ treatment. Data are representative of three technical replicates.
(G) Staining of CD11c (Alexa488, green) and SOCS2 (rhodamine, red) in patient specimens (n = 5-7 patients assayed per group with representative immunofluorescence depicted).
See also Figure S5 and Data S1.

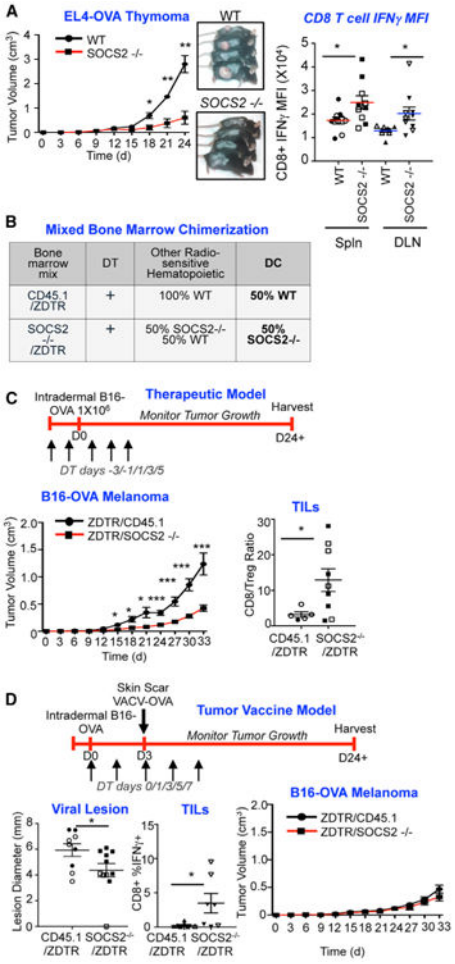

Figure 6. Global and DC-Specific SOCS2 Expression Inhibits Antitumor Immunity

(A) Intradermal growth of EL4-OVA thymoma (left). OVA-peptide-specific $CD8^+$ T cell recall assay. Intracellular cytokine staining of IFNγ in T cells isolated from the spleen and tumor draining LNs of *SOCS2*$^{-/-}$ and WT mice.

(B) Table depicting the breakdown of the immune cells present during use of ZBTB46 (ZDTR) mixed bone marrow chimeras for uncompensated DC-specific loss.

(C) Therapeutic model of acute restriction to *SOCS2*$^{-/-}$ DCs using DT administration surrounding tumor implantation, and concurrent B16-OVA growth with the intratumoral CD8/Treg ratio.

(D) Schema for therapeutic tumor vaccine model. VACV-OVA was administered 3 days after B16-OVA implantation in bone marrow chimera mice and given DT to generate a DC-specific loss of *SOCS2* surrounding implantation. Vaccinia tail lesion diameter (left), frequency of OVA-specific IFNγ + $CD8^+$ TILs assayed by peptide recall and intracellular cytokine staining (middle), and intradermal B16-OVA tumor growth (right). Tumor growth curves were pooled from three independent experiments of four to five mice per group. For antigen recall and TILS analysis, open and closed shapes represent each pooled independent experiment, with individual animals from replicate experiments depicted.

Error bars show mean ± SEM. *p ≤ 0.05; **p ≤ 0.01; ***p ≤ 0.001. See also Figure S6.

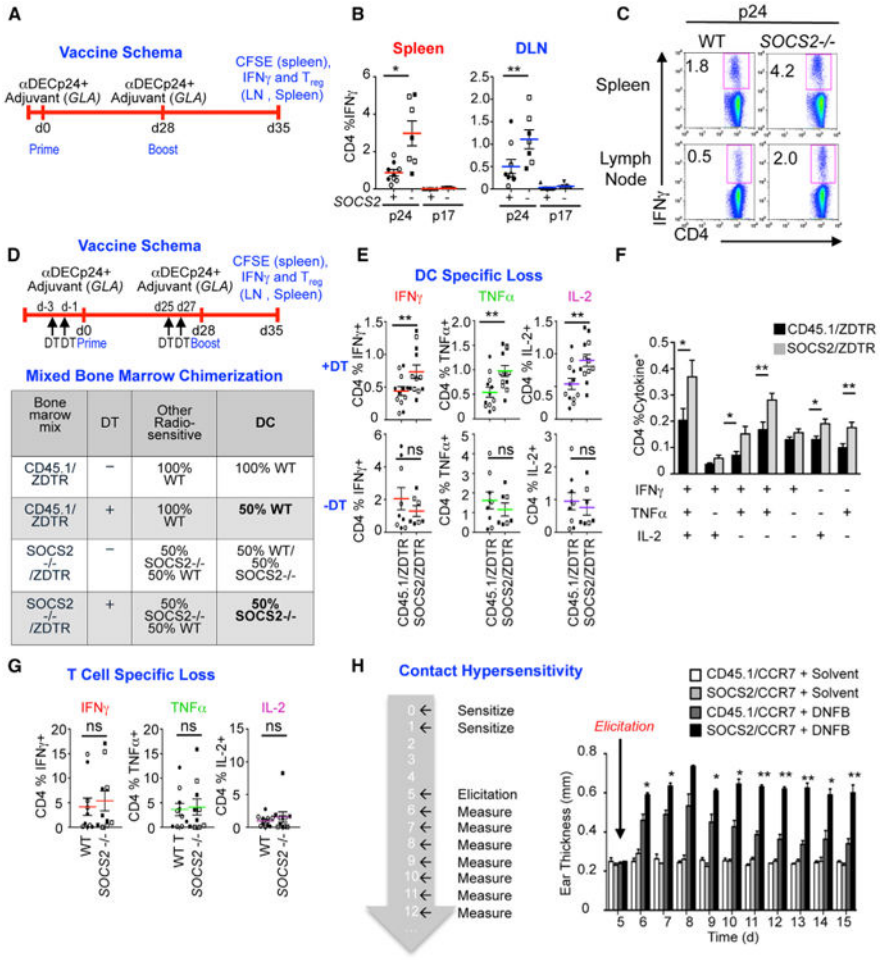

Figure 7. SOCS2 Inhibits Adaptive Immune Priming by DC

(A) Schematic for aCD205-gagp24 protein immunization.

(B and C) (B) Intracellular cytokine staining. HIV gag p24 antigen-specific or control p17 recall IFNγ production by $CD4^+$T cells in WT and *SOCS2*$^{-/-}$ mice1 week after αCD205-gagp24 prime-boost immunization, with (C) representative flow.

(D) Schematic of αCD205-gagp24 protein immunization with diphtheria toxin (DT) administered 1 and 3 days prior to prime and boost. Table depicting the breakdown of the immune cells present during use of ZBTB46 (ZDTR) mixed bone marrow chimeras, +/− diphtheria toxin administration for acute DC-specific loss.

(E and F) (E) Individual or (F) combinatorial expression of IFNγ, TNFα, and IL-2 in HIV gag-p24 specific splenic $CD4^+$ T cells.

(G) *SOCS2*$^{-/-}$ T cells or WT T cells were adoptively transferred into Rag2$^{-/-}$ recipients. One week following boost, intracellular cytokine staining of T cells was performed with HIV gagp24 peptide re-challenge.

(H) Contact sensitivity schema (left) and murine ear thickness (right) following induction of contact hypersensitivity in mice with loss of *SOCS2* restricted to CCR7-dependent cells. Open and closed shapes represent individual animals pooled from each of two independent experiments. All experiments were performed at least twice, with three to six mice per group.

Error bars show mean ± SEM. *p ≤ 0.05, **p ≤ 0.01, ***p ≤ 0.001. See also Figure S7.

Key Resources Table

Reagent or Resource	Source	Identifier
Antibodies		
anti CD3	Thermo Fisher Scientific	eBio500A2
anti CD4	Thermo Fisher Scientific	RM4-5
anti CD8	Thermo Fisher Scientific	53-6.7
anti IFNγ	Biolegend	XMG1.2
anti TNFα	Biolegend	MP6-XT22
anti IL-2	Biolegend	JES6-5H4
anti CD45	Biolegend	30-F11
anti CD11b	Biolegend	M1/70
anti B220	Biolegend	RA3-6B2
anti CD19	Thermo Fisher Scientific	eBio1D3
anti NK1.1	Thermo Fisher Scientific	PK136
anti FoxP3	Ebiosciences (kit)	FJK-16S
anti IAIE	Biolegend	M5/114.15.2
Live/dead AQUA	Molecular Probes, Life Technologies	Cat #: L34966
Anti SOCS2	Abcam (western blot)	Cat #: ab3692
Anti- beta actin	Sigma (western blot)	AC-15
anti BDCA1	Thermo Fisher Scientific	L161
anti BDCA3	Miltenyibiotec	AD5-14H12
anti CD20	Biolegend	2H7
anti CD66b	Biolegend	G10F5
anti CD56	BD Biosciences	NCAM16.2
anti CD11c	Biolegend	B-ly6
anti CD14	Beckman Coulter	RM052
anti CD45	Biolegend	HI30
anti HLA	BD Biosciences	L243
anti-SOCS2	LifeSpan Biosciences- immunofluorescence use	EPR2588(2)
Bacterial and Virus Strains		
Vaccinia-OVA	Jonathon Yewdell laboratory	N/A
Biological Samples		
Human primary melanoma, dysplastic nevi, common nevi, healthy skin	Krueger Laboratory	N/A
Chemicals, Peptides, and Recombinant Proteins		
dinitrofluorobenzene	Sigma	Cat#: D1529-10ML
Diphtheria toxin	Sigma	Cat #: D0564-1MG
Deposited Data		
IFNGR1$^{-/-}$, C57BL6/J WT, IL27Ra$^{-/-}$ skin migratory DCs	Sorted migratory DCs from the skin draining LN; sorted IAIE high CD11c intermediate from all strains	GEO: GSE98994

Reagent or Resource	Source	Identifier
Normal human skin and primary human melanoma	Human skin biopsy specimens	GEO: GSE100050
Single-cell sequencing data human melanoma	BDCA1^{+} BDCA3^{+} and CD14^{+} monocyte populations isolated from a single LN melanoma metastasis	Newly deposited dbGAP, accession pending. Processed single-cell and bulk RNA-seq data is available at GEO: GSE######.
Experimental Models: Cell Lines		
B16-OVA	Arlene Sharpe Laboratory- *mycoplasm testing done in Anandasabapathy lab*	N/A
EL-4 OVA	Charles Drake Laboratory- *mycoplasm testing done in Anandasabapathy lab*	N/A
Experimental Models: Organisms/Strains		
C57Bl6/J	Jackson Labs	Stock No: 000664
IFNGR1$^{-/-}$	Jackson Labs	Stock No: 003288
IL-27Ra$^{-/-}$	Quintana Laboratory; available Jackson Labs	Stock No: 018078
SOCS2$^{-/-}$ mice	Doug Hilton and Warren Alexander Laboratory	Walter and Eliza Hall Institute of Medical Research
CCR7$^{-/-}$	Bred locally and available Jackson Labs	Stock No: 006621 Martin Lipp, Max-Delbrueck-Center
ZBTB46-DTR	Bred locally and available Jackson Labs	Nussenzweig Lab source; Stock No: 019506
Software and Algorithms		
R v 3.3.2, R code available upon request	Mayte Suarez-Farinas	N/A
Other code available upon request	Shalek, Regev, and Troyanskaya Labs	N/A